 Open access • Posted Content • DOI:10.5281/ZENODO.5149023

Assembled chromosomes of the blood fluke *Schistosoma mansoni* provide insight into the evolution of its ZW sex-determination system — [Source link](#)

[Sarah K. Buddenberg](#), [Sarah K. Buddenberg](#), [Alan Tracey](#), [Duncan Berger](#) ...+12 more authors

Institutions: [Morgridge Institute for Research](#), [Wellcome Trust Sanger Institute](#), [University of Liverpool](#)

Published on: 10 Jul 2021 - [bioRxiv](#) (Cold Spring Harbor Laboratory)

Topics: [Pseudoautosomal region](#), [ZW sex-determination system](#), [Pseudogene](#), [Genome](#) and [Synteny](#)

Related papers:

- [Miniscule differences between sex chromosomes in the giant genome of a salamander](#)
- [The Gene Content of Mammalian and Avian Sex Chromosomes](#)
- [Transposable elements and early evolution of sex chromosomes in fish](#)
- [Recurrent gene amplification on Drosophila Y chromosomes suggests cryptic sex chromosome drive is common on young sex chromosomes](#)
- [Single-molecule genome assembly of the Basket Willow, *Salix viminalis*, reveals earliest stages of sex chromosome expansion](#)

Share this paper:    

View more about this paper here: <https://typeset.io/papers/assembled-chromosomes-of-the-blood-fluke-schistosoma-mansoni-1haqw3mv40>

1 Assembled chromosomes of the blood fluke
2 *Schistosoma mansoni* provide insight into the
3 evolution of its ZW sex-determination system

4
5 Sarah K Buddenborg^{1,2*}, Alan Tracey¹, Duncan J Berger¹, Zhigang Lu¹, Stephen R Doyle¹,
6 Beiyuan Fu¹, Fengtang Yang¹, Adam J Reid¹, Faye H Rodgers¹, Gabriel Rinaldi¹, Geetha
7 Sankaranarayanan¹, Ulrike Böhme^{1,3}, Nancy Holroyd¹, Matthew Berriman^{1*}

8
9 ¹ Wellcome Sanger Institute, Wellcome Genome Campus, Hinxton, Cambridgeshire CB10 1SA, UK

10 ² Morgridge Institute for Research, Howard Hughes Medical Institute, University of Wisconsin-Madison, WI, USA

11 ³ Institute of Systems, Molecular and Integrative Biology, University of Liverpool, Liverpool L69 7ZB, UK

12
13 * Corresponding authors

14

15

16

17

18

19 ABSTRACT

20 Background

21 *Schistosoma mansoni* is a flatworm that causes a neglected tropical disease affecting millions
22 worldwide. Most flatworms are hermaphrodites but schistosomes have genotypically
23 determined male (ZZ) and female (ZW) sexes. Sex is essential for pathology and transmission,
24 however, the molecular determinants of sex remain unknown and is limited by poorly resolved
25 sex chromosomes in previous genome assemblies.

26 Results

27 We assembled the 391.4 Mb *S. mansoni* genome into individual, single-scaffold chromosomes,
28 including Z and W. Manual curation resulted in a vastly improved gene annotation, resolved
29 gene and repeat arrays, trans-splicing, and almost all UTRs. The sex chromosomes each
30 comprise pseudoautosomal regions and single sex-specific regions. The Z-specific region
31 contains 932 genes, but on W all but 29 of these genes have been lost and the presence of five
32 pseudogenes indicates that degeneration of W is ongoing. Synteny analysis reveals an ancient
33 chromosomal fusion corresponding to the oldest part of Z, where only a single gene—encoding
34 the large subunit of pre-mRNA splicing factor U2AF—has retained an intact copy on W. The
35 sex-specific copies of U2AF have divergent N-termini and show sex-biased gene expression.

36 Conclusion

37 Our assembly with fully resolved chromosomes provides evidence of an evolutionary path taken
38 to create the Z and W sex chromosomes of schistosomes. Sex-linked divergence of the single
39 U2AF gene, which has been present in the sex-specific regions longer than any other extant
40 gene with distinct male and female specific copies and expression, may have been a pivotal
41 step in the evolution of gonochorism and genotypic sex determination of schistosomes.

42 KEYWORDS

43 sex chromosomes, schistosomiasis, centromere, gametologues, sex determination,
44 gonochorism, sex chromosome evolution, spliced-leader trans-splicing, gene clusters

45 BACKGROUND

46 *Schistosoma mansoni* is one of three main schistosome species that causes schistosomiasis, a
47 neglected tropical disease that affects ~240 million people worldwide [1]. Within the Phylum
48 Platyhelminthes (flatworms), schistosomes are remarkable; while virtually all other flatworm
49 families are hermaphrodites, family schistosomatidae are gonochoristic (separate sexes) and
50 sexually dimorphic as adults. Sex is genetically determined with heterogametic females ($2n=16$,
51 ZW) and homogametic males ($2n=16$, ZZ).

52 Adult female worms reside within the gynecophoric canal of adult males and the paired worms
53 produce several hundred eggs a day. The eggs either traverse the intestinal wall to reach the
54 lumen and be excreted in faeces or become trapped in host tissues, mainly liver and intestine,
55 driving the pathology associated with schistosomiasis [2]. It has been postulated [3,4] that
56 dimorphism and gonochorism in schistosomes is an evolutionary adaptation to their residence
57 in the venous system, close to capillary beds of warm-blooded host species; a division of labor
58 between the sexes enables both a muscular male body to move against the blood flow of large
59 veins and a thin slender female body shape to deposit eggs in small venules, allowing their
60 efficient exit. However, the adaptations required to develop this dimorphism are unclear, limited
61 by a lack of understanding of sex-linked molecular mechanisms, including unresolved sex
62 chromosomes.

63 Despite major advances in the quality and quantity of published genome assemblies, sex
64 chromosomes that are limited to the heterogametic sex (W and Y) are underrepresented in the
65 growing list of whole genome assemblies. These sex-specific chromosomes are usually present

66 at a lower copy number than autosomes, and the problem of assembling them is compounded
67 by difficult to resolve highly repetitive sequences and by genetic divergence between the sex
68 chromosomes, such that they can vary along their lengths [5]. There are exceptions—notably
69 the recent publication of the eel genome [6] included resolved centromeres, subtelomeric
70 sequences and the highly repetitive Y chromosome short arm containing no gaps—but other
71 sex chromosome assemblies, such as the *Drosophila* Y chromosome [7] and *Gallus gallus* W
72 chromosome [8], are in fragmented states and even the reference human Y chromosome
73 assembly [9] lacks continuity between the heterochromatic and euchromatic regions.

74 Degeneration of sex-limited chromosomes (W or Y) often distinguishes them from the shared (Z
75 or X) chromosomes. Along the W chromosome of schistosomes, extensive
76 heterochromatinization and the accumulation of satellite repeats, has been described, including
77 a large satellite repeat SM-alpha [10]. Extensive gene loss, or pseudogene-formation is also
78 expected but without an adequate W assembly, it has not previously been possible to
79 comprehensively describe the W-specific gene and repeat content that may play an important
80 role in sex determination.

81 The *S. mansoni* genome was first published as a draft assembly [11], followed by a more
82 contiguous version (v5) three years later [12] that took advantage of high throughput short-read
83 sequencing technology. At that stage, as much as 80% of the genome had been assigned to
84 chromosomes but gaps were prolific and large regions remained unresolved. The Z and W
85 sequences were assembled together into merged scaffolds, with multiple Z-specific sequences
86 and almost no resolution of W-specific sequences. As part of a sustained commitment to
87 produce a complete genome sequence, in the present study, we have significantly improved
88 upon previous efforts using a combination of long-read sequencing technology, optical mapping
89 and manual curation to generate a highly contiguous chromosome-scale assembly that includes
90 a fully assembled Z chromosome and a contiguous representation of the highly repetitive W
91 chromosome. Our fully resolved reference genome is a key pre-requisite for understanding the

92 evolution of sexual dimorphism in schistosomes and exposes sex-linked protein-coding and
93 non-coding genes tentatively involved in sex determination.

94 RESULTS

95 The chromosome-level genome of *Schistosoma mansoni*

96 Using a combination of PacBio long-read and Illumina short-read sequencing, optical mapping,
97 fluorescent *in situ* hybridization (FISH), Hi-C, and manual curation, we have assembled
98 complete chromosomes from the 391.4 Mb genome of *S. mansoni*, including resolution of its Z
99 and W sex chromosomes. The assemblies of chromosomes 2, 5, 6 and 7 comprise single
100 scaffolds with telomeric repeats at either end; the remaining 5 chromosomes are also single
101 scaffolds with a telomere at one end and sub-telomeric sequence at the other (Figure 1a,b).
102 The number of gaps has decreased by 96% from 8,640 in the previous assembly to just 356
103 (Table 1).

Table 1.

	v5	v9
Assembly size (Mb)	364.5	391.4
Gaps	8,640	356
Repeat Content (Mb)	191.8	213.2
Scaffolds		
Number	885	9
N50 (Mb)	32.1	52.8
N90 (Mb)	0.547	25
Largest (Mb)	65.5	89.1
Gene statistics		
Protein-coding genes	10,116	9,794
Novel genes*	-	810
Deleted genes	-	867
Pfam annotated	66.9%	70.3%

Transcript statistics		
Transcripts	11,075	14,031
Alternative splicing	6.9%	27.9%
Average exons per transcript	5.9	7.9

104

105 The total repeat content of the assembly is 213.2 Mb (Table S1), a 21.4 Mb increase compared

106 with the previously published version [12], reflecting the ability of PacBio long-read sequencing

107 to account for repetitive regions that were previously difficult to assemble. For instance, an

108 array of rRNA genes known as the nucleolar organizer region (NOR) of chromosome 3 (Figure

109 1) was highly collapsed in the earlier assembly and is now fully resolved. Newly resolved

110 repetitive regions also include arrays of tandemly duplicated protein-coding genes enabling us

111 to obtain a more accurate count for genes previously thought to be present as single copies.

112 Two striking examples are the major egg antigens IPSE (IL-4-inducing principle of *S. mansoni*

113 egg) and omega-1. These genes, specifically expressed in the eggs, have been intensely

114 studied due to their roles in immune-modulation, pathogenesis and mechanisms of egg

115 translocation to the intestinal lumen [13–16]. IPSE and omega-1 transcripts are encoded by

116 paralogous gene arrays of at least 13 and 7 gene copies, respectively. In fact, based on the

117 depth of coverage of aligned sequencing reads, these numbers are likely to be even higher and

118 may contain as many as 20 and 14 copies of IPSE and omega-1, respectively (Figure S2).

119 We extended the analysis to identify other clusters of genes with conserved functions. Across

120 the genome, there are 44 clusters of genes sharing similar predicted functions based on their

121 protein (Pfam) domains, more than twice the number of clusters and domain types as seen in

122 the previous v5 published genome version (Table S2). Clusters of *S. mansoni* Kunitz protease

123 inhibitors and elastases are striking. Eleven Kunitz protease inhibitors (PF00014) exist in a

124 cluster and 25 copies of elastase (PF00089; trypsin) are found across two clusters. The well-

125 studied SmKI-1 (Smp_147730 in v5; Smp_311660, Smp_311670, and Smp_337730 in v9), is

126 known to be involved in defense mechanisms of *S. mansoni* within the mammalian host [17].

127 The elastases are an expanded group of serine proteases originally noted for their role in host

128 skin penetration, but are also expressed in intra-molluscan stages, where they likely facilitate
129 movement of the parasite through snail tissue [18,19].

130 Annotation improvements through manual curation

131 We have significantly improved upon previous gene annotations of the *S. mansoni* genome.
132 Using Augustus [20] and extensive RNA-seq evidence (Table S3) for gene prediction, followed
133 by extensive manual curation, the total number of genes has decreased from 10,116 to 9,794
134 (excluding genes on scaffolds that correspond to alternative haplotypes; Table S4), compared
135 to the v5 genome. This is the lowest number of genes for any sequenced platyhelminth; for
136 instance, the cestodes *Echinococcus multilocularis* [21] and *Hymenolepis microstoma* [22] have
137 10,663 and 10,139 genes, respectively. In spite of the modest net reduction in genes, a total of
138 3,610 updates to gene models from v5 to v9 have been made, including 810 new, 867 deleted,
139 344 merged, 189 multiple copies, 190 split, and 1,210 with large structural changes (defined as
140 >20% of coding region affected; Figure S3; Tables S5-S6). Using BUSCO v3.0.2 [23], the *S.*
141 *mansoni* protein set was estimated to be 95.3% complete based on the representation of
142 eukaryota orthologs (full genome-level BUSCO results at Table S7).

143 Spliced leader (SL) trans-splicing is an mRNA maturation process where an independently
144 transcribed SL exon is transferred to a pre-mRNA. SL sequences originate from SL genes 613
145 bp in length, consisting of a 36 bp exon sequence (position 144–181 bp) flanked by an
146 upstream precursor sequence (1–143 bp) and a downstream intron (182–613 bp) (Figure S1).
147 A ~1 Mb tandem array containing 41 full-length spliced-leader (SL) RNA genes has been
148 resolved on chromosome 6 (Figure S1), together with an additional 109 partial gene sequences
149 that contain the exon sequence only in the same array. On most other chromosomes, 1–4 SL
150 gene fragments containing the exon sequence can also be found. Using RNA-seq data from all
151 life cycle stages with an improved gene set (Table S3), we located SL receptor sequences in
152 the transcripts of 6,641 genes in the primary assembly (i.e. no haplotypes), indicating that the
153 majority of genes (66.3%) encode at least one trans-spliced isoform compared to 6.9% reported

154 in the previous assembly (Table S8). This number is similar to the nematode *Caenorhabditis*
155 *elegans* where ~70% are identified as being trans-spliced [24].

156 The complexity of gene structures has increased substantially; the average number of exons
157 per gene has increased from 5.9 to 7.9 (Table 1) and 97.7% of transcripts have both 5' and 3'
158 untranslated regions (UTRs) annotated (Table S9). Further, the proportion of genes with
159 alternative splicing to generate distinct transcribed isoforms has increased from 6.9% to 27.9%.
160 Systematic improvements to gene finding and gene structural changes have enabled a richer
161 set of putative functions to be ascribed to the *S. mansoni* proteome, reflected in the 47 new
162 protein (Pfam) domains to *S. mansoni* from new genes and 79 new Pfams domains annotated
163 in genes with improved gene structure (Table S10).

164 Centromere motif conservation and divergence

165 *S. mansoni* chromosomes are monocentric [25], each with a cytologically distinguishable
166 primary constriction (Figure 1a). The centromeric sequences are large repeat arrays that, on all
167 chromosomes except 4 and Z, are highly conserved within a centromeric array and are
168 between 93.1–98.5% similar to a 123 bp centromeric repeat proposed by Melters et al. [26]
169 (Figure S4; Table S11). Between the centromeres of different chromosomes, the sequence
170 conservation is more variable: 56% identity between the two most divergent centromere
171 monomers (chromosomes Z and 6) and 100% identity between the centromeres of
172 chromosomes 2 and 3 (Figure S4). The unit size is typical of the centromeric repeats of many
173 other species [26], including the platyhelminth *Hymenolepis microstoma* [22]. The centromeric
174 repeats for chromosomes 4 and Z have diverged from each other and from those of other
175 chromosomes (Figure S4); their respective repeat units are 107 and 175 bp, and they are only
176 82 and 59% identical to the consensus from Melters et al. Centromeric repeats were previously
177 estimated to comprise 0.48% of the genome (1.9 Mb) [26], but after including the divergent
178 centromeres and estimating the degree to which all centromeric repeats were under-
179 represented in the assembly based on mapped sequence coverage (from three PCR-free

180 Illumina libraries), we estimate that centromeres make up at least 1.15% (4.5 Mb) of the
181 genome.

182 Architecture of the Z chromosome

183 Our new assembly includes a full-length 88 Mb Z chromosome that includes defined,
184 recombining pseudoautosomal regions 1 (10.7 Mb) and 2 (42.9 Mb) and a non-recombining
185 33.1 Mb Z-specific region. In contrast to the previously published v5 assembly [12], where the Z
186 chromosome was only partially resolved, the new sequence is 27.2 Mb larger with
187 misassemblies corrected along its length, aided by the new long-range information that has
188 been incorporated (Figure 2). In particular, the sequence that is unique to the Z chromosome
189 (i.e., the Z-specific region, or ZSR), is clearly visible based on the lower depth of coverage of
190 resequencing reads mapped from heterogametic females. The ZSR is flanked by two regions
191 that are common to both sex chromosomes, termed pseudoautosomal region (PAR) 1 and 2.
192 Based on the earlier assembly (v5), it was previously shown [27] that the Z chromosome
193 comprises different sub-regions or strata that have evolved differentially in the African and
194 Asian *Schistosoma* lineages from a common ‘Ancestral’ stratum that is common to both
195 lineages. Using the v9 assembly as a reference, where the ZSR is now resolved as a 33.2 Mb
196 continuous sequence (Figure 2; Table S12), we plotted coverage of mapped sequencing reads
197 across Z chromosome orthologs from four schistosome species (*S. mansoni*, *S. rodhaini*, *S.*
198 *haematobium*, *S. japonicum*) and the hermaphroditic trematode *Echinostoma caproni*. In
199 contrast to the relatively uniform mapped coverage for *E. caproni*, the ZSRs for the
200 *Schistosoma* species are clearly visible, with a 19.1 Mb Ancestral shared region (ZSR2; ZSR
201 coordinates 13,993,393-33,063,208) that has extended more recently in different directions
202 amongst the African (*S. haematobium*, *S. rodhaini*, *S. mansoni*) and Asian species (*S.*
203 *japonicum*). It also appears that in the Asian *S. japonicum*, two inversions have resulted in
204 orthologues changing position and, therefore, creating coverage anomalies near the ZSR
205 boundaries. The more recent 14 Mb African stratum (ZSR1; ZSR coordinates 1 - 13,993,392)

206 extends beyond the centromere but is shorter than the Ancestral stratum (ZSR2). In contrast to
207 the single, contiguous Z-specific region in the v9 assembly, the v5 assembly contained two
208 blocks of what we now know to be PAR fragments which were incorrectly located inside the
209 sex-specific region. It was previously reported that blocks of sequence shared by Z and W are
210 located in the large region of recombination repression (i.e. the ZSR) [28]; based on this
211 observation, Hirai, Hirai, and LoVerde [29] proposed three inversions in homologous Z/W
212 regions from Z to W occurred before heterochromatinization, followed by at least one more
213 inversion. These conclusions do not hold true in v9 and can now be attributed to misassemblies
214 in v5.

215 To gain further insight into the evolutionary origins of the ZSR, we looked at the relationship
216 between the Z chromosome and the chromosomal sequences of distantly related tapeworms.
217 We have previously shown that flatworm genome structure can be defined based on conserved
218 chromosome synteny blocks [30] (Figure 3b). When orthologs of *S. mansoni* and tapeworms
219 are compared, synteny is largely preserved between these blocks, even though collinearity is
220 disrupted. It is evident that one end of the Z chromosome is highly related to chromosome 3 of
221 *Echinococcus multilocularis* and the other end is highly related to chromosome 5. When taken
222 in isolation, the orthology evidence equally supports an ancient fusion in the schistosome
223 lineage or an ancient fission in the tapeworm lineage. However, the position of the junction
224 between the chromosome synteny blocks coincides with the position of the Ancient stratum
225 (Figure 3a), suggesting that a fusion in the schistosome lineage is likely to have played a role,
226 resulting in suppressed recombination.

227 For neutral positions in the genome, the genetic diversity present is expected to reflect the
228 number of copies of that region in the genome [31]. For the ZSR, the relative number of copies
229 is 0.75 relative to autosomes (1.0), thus the diversity is expected to be lower than that of
230 autosomes. Along the ZSR, we identified 352 genes in the African stratum and 580 in the
231 Ancient stratum, which are flanked by 229 and 1,071 protein-coding genes in PAR1 and PAR2,
232 respectively. We calculated the median nucleotide diversity (π) across the protein-coding genes

233 of the autosomes and PARs and Z-specific regions (Figure 4; Table S13) using published
234 genome variation data [32]. Across 50 kb windows, the autosomes have a median π range of
235 0.0026 to 0.0039. The PARs have a similar median π range to that of the autosomes at 0.0027
236 to 0.0032 in females and 0.0027 to 0.0034 in males suggesting that recombination between ZW
237 and ZZ bivalents in the PARs is similar to that of the autosomal chromosomes. Also, the median
238 π of the ZSR is significantly lower than that of the PARs for both males and females ($p < 0.001$;
239 Mann-Whitney test). We observed significantly lower π values in the Z African stratum when
240 compared to the Z Ancestral stratum in both male and female samples ($p < 0.001$; Mann-Whitney
241 test), consistent with the effective population size of the Ancestral stratum being smaller for
242 longer. The π values of the Z chromosome are close to that which would be expected in a
243 neutral equilibrium with equal and constant male and female populations sizes
244 ($\pi_Z/\pi_{Autosomes}=0.75$; [31] with $\pi_Z/\pi_{Autosomes}=0.71$ in males and $\pi_Z/\pi_{Autosomes}=0.70$ in females.

245 Assembling the W Chromosome

246 The W chromosome shares >50 Mb of sequence with the Z chromosome in the
247 pseudoautosomal regions, PAR1 and PAR2, that flank a highly repetitive W-specific region
248 (WSR) (Figure 5; Table S12). In the v5 assembly, the highly repetitive W-specific region could
249 not be resolved beyond ~100 small and unordered contigs (1.1 Mb); by sequencing clonal
250 females on multiple sequencing platforms, we resolved 22 repeat-rich W-specific scaffolds
251 totalling 3.7 Mb (Figure S5). In many cases, the long reads used in our assembly were
252 insufficient to fully span the arrays of repeats in the W chromosome. As a result, unique
253 sequences are represented but the number of repeat units in many of the repeat arrays is vastly
254 underestimated. After manual curation of the major repeat blocks, the W-specific assembly
255 scaffolds were further ordered, oriented and linked by identifying as few as one, long PacBio
256 subreads that spanned two consecutive blocks (Table S14). Metaphase FISH was also used to
257 localize and orient three W-specific scaffolds that could not be placed through computational
258 assembly methods (Figure S5).

259 Previous karyotype measurements from 22 female metaphase cells [33] showed the W
260 chromosome to be approximately 14% longer than the Z chromosome, a figure we confirmed
261 with our own measurements of 14.7% using 6 female metaphase cells (Table S15; Figure S6).
262 In particular, a long repetitive region in the short (p) arm of the W chromosome accounts for
263 much of this size difference and is responsible for the p-arm being ~40% of the W-chromosome
264 length. Assuming a uniform density along the chromosome, relative measured lengths of other
265 chromosomes with known assembly sizes (Figure S6), and genomic coverage of W-specific
266 repeats (Table S16), we estimate the size of the W-specific region (WSR) to be ~46 Mb.
267 However, given that this region is heterochromatic and, therefore, more densely packed, its true
268 size could be much longer. We attempted to estimate the degree to which repetitive regions
269 remain collapsed within the assembly by mapping high-coverage Illumina sequencing reads
270 from adult females. Extrapolating the read depth across repetitive regions (Table S16; see next
271 section for results on W repeats) and comparing it with the median coverage for the genome
272 (Table S17; ERS039722), we estimate a length of 17.6 Mb for the W-specific region. Clearly the
273 mapping approach is inaccurate for estimating the true size of these collapsed regions. In fact,
274 there are many regions of repetitive sequence in W where very few Illumina reads are mapped,
275 indicating that certain repeat motifs are underrepresented in the sequence data. So-called
276 “dark” and “camouflaged” regions of genomes have previously been reported, where specific
277 sequencing technologies perform poorly (e.g. short tandem repeats, duplicated regions, regions
278 with high GC content, non-random fragmentation) [34,35].

279 Repeat classification and heterochromatinization of the W 280 chromosome

281 Like the human Y chromosome, the *S. mansoni* W chromosome is largely heterochromatic with
282 a large proportion of its length composed of satellite repeats. There are just three bands of
283 euchromatin on the W chromosome (chevrons in Figure 5) [10,33]. Because some individual
284 PacBio reads contained tandem arrays of the same repeat unit, we were able to assemble

285 complete repeat units. Within the WSR constitutive heterochromatin, we characterized 36
286 unique repeats, named smw01-smw36 (Figure 5; Table S16). The 36 W-specific repeats
287 comprise >95% of the assembled length of the W-specific region.

288 Of the 36 repeats, five (smw07, smw20, smw21, smw25, smw29) are related to the previously
289 described 337 bp retrotransposable element SM α t-2 [36,37]. Although a variant of SM α t-2 has
290 been previously published as female-specific (SMAlpha-fem-1; NCBI accession U12442), we
291 found one complete copy (coordinates: 23,37,004–23,936,670; 92.3% identity, 99.7%
292 coverage, e-value 9.07e-133) and 38 partial copies (>75.0% identity; >95.0% coverage) on the
293 Z chromosome. Metaphase FISH has shown striking fluorescence of a SM α t-2-related probe
294 hybridizing near the short arm euchromatic gap [33,37]. However, across the v9 genome, we
295 found SM α t-2 repeats sporadically distributed on all autosomes and both sex chromosomes
296 [38], but only as a large tandem array on the W chromosome, corresponding to the smw07
297 repeat found near the euchromatic band of the short arm [33].

298 Interestingly, 21 of the repeats can be grouped into five distinct families, where members within
299 each family share at least 75.0% nucleotide identity, suggesting they may have evolved from a
300 common ancestor including an SM α (aka SM-alpha and SMApha-fem) retrotransposon repeat
301 family (smw03, 07, 20, 21, 29) (Table S16).

302 Gametologues and their possible role in schistosome sex 303 determination

304 The ZSR contains a total of 932 protein-coding genes. Of these, only 33 have clear
305 homologous copies (termed gametologues) on the W chromosome, all within the WSR (Table
306 S18). Although there is some positional clustering, extensive rearrangements by inversions,
307 repeat expansions and transposable elements have largely disrupted collinearity between the
308 WSR and the ZSR. The more recent African stratum contains 31 of the gametologues. For two
309 of these, the corresponding W-copies have duplicated; there are three copies of genes

310 encoding DnaJ domain proteins (heat shock protein 40 member B6) and two copies encoding a
311 hypothetical protein with no discernible conserved features. At least five of the gametologues in
312 the African stratum have degenerated into pseudogenes on W that have not yet been lost.

313 Considering the longest transcript for each gene, the W gametologues have an average of 55
314 amino acids less per protein sequence than the Z gametologues (Table S19). Only three W
315 gametologues (spliceosome-associated protein, Smp_310950; ENTH domain-containing
316 protein, Smp_303540; splicing factor U2AF 35 kDa small subunit, Smp_348830) are longer
317 than their Z counterparts. Most Z and W gametologues are highly similar with average amino
318 acid identities of >80% across their entire lengths using the Needle Wunsch algorithm in the
319 EMBOSS package [39]. Excluding the five W pseudogenes and their Z gametologues, the
320 gametologue pair with the greatest divergence was Smp_348820 on W and Smp_031310 on Z
321 (encoding 40S ribosomal subunit S26) with only 47.6% identity. However, as with other low-
322 similarity pairs, it was not possible, even through manual curation, to rule out gene finding
323 inaccuracies due to a lack of isoform-specific transcript data.

324 We used previously published sex- and stage-specific RNA-seq [40,41] to analyse differences
325 in expression between the Z and W gametologue pairs (Figure 6). As expected, using unique
326 mapping reads only for analysis, very few male reads mapped to the W gametologues. There
327 were slight differences in the levels of expression between male and female samples for the Z
328 gametologues, although RNA-seq coverage and replicate number from some of these samples
329 were inadequate to enable robust analysis and interpretation. It has been shown one
330 gametologue pair, encoding DnaJ homolog subfamily B member 4, have diel expression in
331 males and females with the Z gametologue (Smp_336770) with the the Z gametologue cycling
332 in adult females, males, and male heads, and the W gametologue (Smp_020920) cycling in
333 females [42]. Expression of several W gametologues in female samples indicates possible
334 stage-specific activity (such as Smp_317860, DnaJ heat shock protein family member B6) that
335 is expressed in female larval cercariae and pre-dimorphic mammalian-stage schistosomula but

336 not in adults; however, the Z gametologue to this gene, Smp_022330, shows consistent
337 expression values across all stages.

338 There is an almost complete lack of gametologues in the Ancestral stratum, which is consistent
339 with this part of the chromosome having become sexually differentiated earlier and
340 degenerative processes thus having been underway for longer. Within this long tract of
341 degenerated sequence, two gametologues are clear exceptions. The first of these is a long
342 multi-exon gene on Z, encoding a protein with ankyrin repeats and helicase domains. The
343 corresponding gametologue on W is a pseudogene with several frameshifts and missing exons
344 (Figure S7a). The second gametologue is predicted to encode the large subunit of splicing
345 factor U2 snRNP auxiliary factor (Smp_019690 on Z and Smp_348790 on W). Strikingly, the
346 sequences are almost identical (>95%) for most of their lengths but have divergent N-terminal
347 sequences. After correcting for an artifactual frameshift in the W chromosome consensus
348 sequence (based on aligned RNA-seq reads; Figure S7b), the copy on W shares the single-
349 exon structure but the first 125 aa share only 45% identity.

350 DISCUSSION

351 Our chromosome-scale assembly and curated annotation significantly extends the genetic
352 resources for *S. mansoni*, and provides a more robust scaffold for genome-wide and functional
353 genomic approaches for this important but neglected pathogen. It has enabled a greatly
354 improved definition of the gene content, with the sequences of more than 25% of genes
355 changed with >20% of coding region affected, and better resolution of those present in
356 repetitive arrays, such as those encoding spliced leader RNA and stage-specific gene families.
357 Amongst the gene families, many are known to encode highly abundant products —such as
358 IPSE, omega-1, elastases, Kunitz protease inhibitors—that are important in host-parasite
359 interactions. Major egg antigens omega-1 and IPSE are associated with a Th2 immune
360 response in the host resulting in granulomatous inflammation around trapped parasite eggs

361 [43]. Given the critical role of the intestinal granuloma for the egg translocation from the blood
362 vessels to the intestinal lumen [44], genome expansions of these genes might have
363 represented a selective advantage.

364 A major advance is in the analysis of schistosome sex chromosome evolution. Our previous
365 analysis of orthologue synteny across the flatworms showed that the *S. mansoni* Z
366 chromosome corresponds to two or more chromosomes in tapeworms [30]. From those data
367 alone, it was not possible to determine whether a chromosome fusion had occurred in the
368 schistosome lineage or whether it was a fission in tapeworms. However, in several other taxa,
369 including filarial nematodes and several lepidoptera, a chromosomal fusion has underpinned the
370 genesis of sex chromosomes [45,46]. We therefore speculate that a fusion has similarly
371 occurred in the ancestral schistosome, creating a new pre-sex autosomal chromosome. The
372 fusion event could have resulted in an isolated sex-determining locus that was advantageous to
373 females and/or antagonistic to hermaphrodite worms. Consistent with this hypothesis, we show
374 that the position of the putative fusion is within the oldest part of the Z-specific region of the
375 chromosome and, within it, there is a single protein-coding ancestral gene (U2AF; splicing
376 factor U2AF 65 kDa subunit) and a single pseudogene that are common to all African and Asian
377 schistosomes. The alternative hypothesis to explain the observed synteny would require a
378 fission at that position somewhere in the tapeworm lineage. This would have occurred prior to
379 the formation of a sex determining region and the fission would, therefore, have played no role.

380 As one of two genomes found in the earliest-diverging part of the sex chromosomes, we identify
381 the W gametologue encoding the pre-mRNA splicing factor U2AF 65 kDa subunit
382 (Smp_348790) as a leading candidate gene for involvement in schistosome sex-determination.
383 U2AF has been studied extensively in *Drosophila* for its association with the master sex-
384 determining protein Sex-lethal (Sxl) [51] that is expressed exclusively in female flies. Sxl
385 competes with U2AF binding to inhibit the splicing and translation of the *msl-2* gene (male-
386 specific-lethal-2) [52,53]. Considering that sex is determined by inhibition of U2AF binding to
387 pre-mRNA in *Drosophila*, it is tempting to speculate that the *S. mansoni* female-specific W copy

388 of U2AF may antagonise the activity of the Z copy to inhibit the splicing of one or more genes.
389 Further implicating U2AF in sex determination, the sex-specific regions also contain a homolog
390 of the U2AF 35kDa subunit. In many taxa, U2AF is a heterodimer composed of large and small
391 subunits that are required for spliceosome assembly in order to remove intron sequences from
392 pre-mRNAs. U2AF binds to the 3' splice site and polypyrimidine tract of introns in a complex
393 with several other small nucleolar ribonucleoproteins (snRNPs) bound to the 5' splice donor,
394 committing pre-mRNA to splicing (see review [50]). Our identification of U2AF2 is independently
395 validated by Elkrewi et al. [49], who show using a search strategy based on the differential
396 distribution of k-mers, that U2AF2 is the only intact gene in the ancient stratum of the ZSR.

397 How has sexual dimorphism evolved in schistosomatidae? The characterization of
398 chromosomal fusions resulting the sex chromosomes, distinct evolutionary strata among closely
399 related species, and the identification of U2AF allows us to propose a model of a model of the
400 evolution of the schistosome sex chromosomes (Figure 8). At some point during the evolution
401 of the Z and W sex chromosomes, the centromeric repeats diverged. It is not possible to know
402 whether the centromere divergence occurred simply as a result of recombination or whether it
403 played a more pivotal role in driving the suppression of recombination. Given the location of the
404 centromere towards the far end of the more recent African stratum of the ZSR, the centromere
405 divergence could have enabled a large expansion of the ZSR in the common ancestor of the
406 African lineage of parasites. The high homology in amino acid sequence along with the
407 conservation of functional domains between the gametologues suggests function has not
408 changed between the gametologue pairs. Analysis of existing RNA-seq revealed sex- and
409 stage-specific expression of the Z and W gametologues that could play a role in female-specific
410 development. The duplication and triplication of two Z gametologues on W may be important in
411 maintaining gene dosage or specialized female expression for those genes and is worthy of
412 future study.

413 Although sexual dimorphism needs not rely on the existence of sex chromosomes and not all
414 sexually dimorphic traits need to be linked to sex chromosomes [55], there must have been

415 selective pressure to isolate sexually antagonistic and/or advantageous loci on non-
416 recombining regions of sex chromosomes [56,57]. Unlike many species in which a master sex-
417 determining gene triggers male or female development, the absence of a W chromosome-
418 specific genes suggests that multiple sex-determining loci were isolated on the sex
419 chromosomes to produce separate sexes. With this in mind, we hypothesize that the W-copy of
420 U2AF is regulating other gametologues or even genes located on the autosomes to control the
421 suppression of male or female function. Identifying downstream interactions of U2AF with other
422 genes is a critical next step for uncovering the mechanisms involved in schistosome sex
423 determination. For example, do posttranslational modifications or splicing of W gametologues
424 by U2AF directly inhibit the activity of a male-promoting product or create a male-lethal product?
425 Future studies are needed to understand the functional role the gametologues like U2AF play in
426 schistosome sex biology.

427 CONCLUSIONS

428 *S. mansoni* is the most studied trematode and an accurate genome sequence underpins
429 research into this important pathogen as well as enabling it to serve as a model for other
430 trematodes. As the first species with completely assembled Z and W sex chromosomes, the *S.*
431 *mansoni* genome provides a novel resource for studying other ZW organisms and is a crucial
432 resource for future investigation into the sexual biology of schistosomes. The results presented
433 provide a significant advance toward understanding the evolution of sex chromosomes among
434 the Schistosomatidae. As the agent of a prominent neglected tropical disease, understanding
435 the evolutionary origins and molecular mechanism of sex determination in schistosomes may
436 reveal new vulnerabilities to combat these parasites. The identification of the W-copy of U2AF
437 as a candidate sex determining factor is clearly a major first step. This new assembly and
438 annotation has already assisted in a broad range of studies on schistosomiasis including
439 monitoring genetic diversity in field strains [32,58], the discovery of alleles under selection for
440 resistance to the antihelmintic praziquantel [59], and the analysis of stage- and sex-specific

441 epigenetic changes [60–62]. Future studies using this resource will undoubtedly continue to
442 reveal novel biological insights into schistosome development, infection, host-parasite
443 interactions, and pathogenicity.

444 METHODS

445 Parasite material

446 *Schistosoma mansoni* developmental stages

447 A summary of the parasite material for genome and transcriptome sequencing can be found in
448 Table S17 and Table S3, respectively. Unless otherwise specified, the different *S. mansoni*
449 developmental stages were collected following described protocols [63,64]. Unless otherwise
450 noted, samples for RNA extraction were resuspended in 1 ml of TRIzol and stored at -80°C until
451 a standard TRIzol RNA extraction method was performed. Genomic DNA was extracted using a
452 standard phenol:chloroform DNA extraction method.

453 Sporocysts

454 Sporocysts were collected from Brazilian *B. glabrata* snails (BgBre) infected with 10 miracidia of
455 their sympatric Brazilian *S. mansoni* (SmBre) strain. Secondary (daughter) sporocysts were
456 dissected from 20 snails at 15 days and 4.5 weeks after infection. Following RNA extraction,
457 DNA was removed with the Ambion® DNA-free™ Kit following the standard procedure and
458 purified with the RNeasy® Mini Kit (QIAGEN).

459 Cercariae

460 At 4.5 weeks post exposure to 15-30 miracidia each, snails were washed, transferred to a
461 beaker containing ~50 ml conditioned water, and placed under light to induce cercarial

462 shedding. Cercariae were collected and water was replaced every 30 minutes for 2 hours.

463 Cercariae were incubated on ice for 30 minutes and concentrated by centrifugation at 1500 x g
464 for 30 minutes at 4°C.

465 Snails exposed to single miracidium each were tested for patent infection after 5 weeks by
466 exposure to light to collect genomic DNA from pooled male and pooled female cercariae. Snails
467 with patent infection were kept and exposed to light every three days. Cercariae collected from
468 each snail were stored for DNA extraction. Sex of the cercariae was identified by PCR [65].

469 Schistosomula and adult worms

470 Briefly, water containing cercariae was filtered, cercariae were washed, and tails were sheared
471 off by ~20 passes through a 22-G emulsifying needle. Schistosomula bodies were separated
472 from the sheared tails by Percoll gradient centrifugation, washed, and cultured at 37°C under
473 5% CO₂.

474 Adult worms were collected by portal perfusion from experimentally-infected mice at 6, 13, 17,
475 21, 28 and 35 days post infection following methods previously described [66]. Clonal female or
476 male adult worms were collected from mice infected with PCR-confirmed female or male
477 cercariae, respectively, shed from single monomiracidium-infected snails.

478 For RNA preparation, samples were thawed on ice and transferred to MagNA Lyser Green
479 Beads (Roche Molecular Systems, Inc). The samples were homogenized using the FastPrep-24
480 instrument (MB Biomedicals, UK) for two 20 second pulses with a speed setting of 6. A
481 standard TRIzol RNA extraction followed and RNA was concentrated using RNA Clean and
482 Concentrator Kit (Zymo Research) according to the manufacturer's recommendations. RNA
483 quality was assessed on the Bioanalyzer (Agilent) and samples with the highest quality were
484 chosen for reverse transcription.

485 Miracidia

486 Livers were removed from hamsters 49 days post-infection with cercariae of the Liberian strain
487 of *S. mansoni* and homogenised in PBS. The homogenate was centrifuged for 10 minutes at
488 5,500 x g at 4°C and the supernatant was discarded. The pellet was washed twice by
489 resuspension in 0.9% NaCl followed by centrifugation as above. The pellet was resuspended in
490 fresh conditioned water, exposed to light, and miracidia were collected. Miracidia were
491 centrifuged for 30 minutes at 15,000 rpm at 4°C. Pelleted miracidia were resuspended in 100 µl
492 TriFast (Peqlab) before storage at -80°C. The miracidia were allowed to thaw at room
493 temperature before homogenisation with a polypropylene pestle, and snap frozen in liquid
494 nitrogen. This was repeated twice more before TriFast was added to 500 µl. RNA was then
495 extracted according to the manufacturer's instructions. Extracted RNA was quantified using a
496 BioPhotometer plus (Eppendorf). RNA quality was assessed with the Bioanalyzer RNA 600
497 Pico Kit (Agilent).

498 Illumina and PacBio genome sequencing

499 Clonal male and female mate pair libraries (3 kb fragment size) were prepared from cercariae
500 genomic DNA, following a modified SOLiD 5500 protocol adapted for Illumina sequencing [67].
501 Additionally, genomic DNA from clonal male and clonal female adult material was used to make
502 separate PCR-free 400-550 bp Illumina libraries following previously described protocols [68],
503 with the exception of using Agencourt AMPure XP beads for sample clean-up and size
504 selection. Genomic DNA was precipitated onto beads after each enzymatic stage with an equal
505 volume of 20% polyethylene glycol 6000 and 2.5 M sodium chloride solution. Beads were not
506 separated from the sample throughout the process until after the adapter ligation stage. Fresh
507 beads were then used for final size selection. Illumina libraries were sequenced on either a
508 HiSeq 2000 or 2500 (Table S17).

509 Genomic DNA from *S. mansoni* clonal female adults was used to prepare a SMRTbell library
510 following the Pacific Biosciences protocol '20 kb Template Preparation Using BluePippin Size-
511 selection System'. The resulting library was used to produce 40 SMRT cells on the Pacific
512 Biosciences RSII platform. We also prepared a PacBio library using genomic DNA from a pool
513 of male cercariae from a snail monomiracidium-infection producing 28 SMRT cells on the
514 Pacific Biosciences RSII platform (Table S17).

515 Optical mapping for genome assembly corrections and increased
516 resolution

517 Female clonal cercariae were used to make agarose plugs using the CHEF Genomic DNA Plug
518 Kit (Bio-Rad) following methods previously described [69]. High molecular weight *S. mansoni*
519 genomic DNA was prepared by proteinase K lysis of trypsin-digested adults mixed with molten
520 agarose set in plugs. DNA molecules were stretched and immobilized along microfluidic
521 channels before digestion with the restriction endonucleases *BamHI* and *NheI*, yielding a set of
522 ordered restriction fragments in the order that they occur within the genome.

523 The optical data was generated and analysed using the Argus Optical Mapping System from
524 OpGen and associated MapManager and MapSolver software tools. As the *S. mansoni*
525 genome is significantly larger than the 100 Mb cut-off suggested by OpGen for *de novo*
526 assembly, OpGen's GenomeBuilder software was used to generate targeted local optical map
527 assemblies from the sequence contigs to provide additional mapping information. The median
528 coverage of fluorescently-labelled molecules in the optical contigs from which consensus
529 sequences were built was 30x. The raw data for each optical map contig were manually
530 scrutinized using OpGen's AssemblyViewer software, allowing us to validate accuracy (i.e.
531 consistent coverage of $\geq 20x$). Contigs with a visible dip in raw molecular coverage were

532 discarded as assembly errors. This resulted in a set of manually curated, non-redundant optical
533 contig consensus sequences that were generated near remaining scaffold gaps, rather than
534 being generated to cover the whole genome, due to finite computational and analytical
535 resources. Comparison of sequence contigs with validated optical contig consensus sequences
536 allowed further scaffolding of the genome assembly and resolution of misassemblies as
537 necessary in Gap5.

538 *de novo* assemblies and manual curation

539 We combined existing short read data [11,12] with additional Illumina data, long PacBio reads
540 (Table S17), optical contigs, and genetic markers [70], to construct an intermediary genome
541 assembly (version 7; GCA_000237925.3) that could be used by the public immediately while
542 time-intensive manual curation took place. Misassemblies were corrected using long-read
543 evidence, as well as optical map data and genetic markers [70]. Remaining gaps were filled
544 using gap-filling software [71,72]. Genetic markers [70] and an updated genetic linkage
545 map(unpublished data, Chevalier et al) were used to assign further scaffolds to chromosomes,
546 and to aid improvement and validation of the rest of the assembly. Version 7 contains 10
547 chromosomal scaffolds (8 chromosomes plus two scaffolds whose coordinates are known in the
548 W chromosome; 95.91% of scaffolded bases), 13 scaffolds assigned to an autosome with
549 known coordinates (11 of these are primarily repetitive scaffolds), 20 W-specific scaffolds
550 without chromosomal coordinates, 17 scaffolds not assigned to a chromosome, and one
551 mitochondrial scaffold.

552 Following the v7 assembly submission, we further improved the assembly, particularly in
553 assembling all W-specific contigs and in creating individual chromosomal scaffolds for both Z
554 and W sex chromosomes. To assemble the W chromosome, we first produced separate *de*

555 *novo* assemblies for Illumina and then used Spades [73]) and CANU [74]) to assemble PacBio
556 genomic reads that did not map to the v7 assembly with >500bp of soft-clipping. Second, the *de*
557 *novo* assemblies were screened against the NCBI NR database in order to screen out any non-
558 *S. mansoni* sequences. New contigs were examined in Gap5 [75] for absence of mapped reads
559 from a male Illumina library (PCR-free pooled male cercariae) and presence of mapped reads
560 from the PCR-free pooled female cercariae Illumina library (Table S17). Manual improvement
561 was performed in Gap5 [75]. Putative new W-specific contigs were examined for sequence
562 similarity to the 22 existing W-specific scaffolds in v7 to determine unique W-specific contigs. All
563 genomic reads (Table S17) were re-mapped to the new assembly and concordant soft-clipped
564 sequences were extended. This process was continued iteratively until no further progress
565 could be made, by which point all contigs terminated in tandem repeats. At this point, the
566 PacBio subreads were surveyed to find long read evidence linking the W chromosome tandem
567 repeats together (Table S16). This elucidated the order of the repeats and W-specific regions to
568 construct a single W chromosome scaffold.

569 Z and W-specific chromosomal regions were determined from mapping coverage of PCR-free
570 female Illumina libraries (Table S17) with ~22x coverage in the ZSR and ~44x coverage in the
571 PARs, as expected in ZW females. Female-only libraries were used to manually identify
572 gametologues on the W chromosome.

573 We resolved the haplotypic diversity that typically exists in genome assemblies by sequencing
574 clonal parasites derived from single miracidium-infected snails. Haplotype genes were
575 determined in Gap5 [75] by identifying genes with half coverage, and localisation to a single
576 scaffold that is also half coverage, as compared to non-haplotype scaffolds. An erroneously
577 classified W chromosome scaffold (SM_V7_W019) from v7 was re-classified as a chromosome
578 1 haplotype. Haplotypes are represented in 259 scaffolds (2.74% of scaffolded bases) (Table
579 S4; DOI:10.5281/zenodo.5149023).

580

581 Metaphase fluorescent *in situ* hybridization (FISH) to confirm order of W-
582 specific scaffolds

583 *S. mansoni* NMRI strain daughter sporocysts from *B. glabrata* snails were dissected at 29 days
584 post exposure. Sporocysts were placed in 0.05% (0.5mg/ml) colchicine (Sigma-Aldrich) and
585 titrated ~20 times using an 18G blunt-end needle. This single cell suspension was incubated
586 at room temperature for 2-4 hrs to arrest cell division. Cells were spun at 500 x g for 5 min,
587 incubated in nuclease-free water for 20 min at room temperature, and then preserved in ice-
588 cold 3:1 methanol:acetic acid fixative.

589 Several primer sets were designed to amplify 15 kb-30 kb fragments using the 22 W-specific
590 scaffolds identified post-v7. Fragments were amplified using either PrimeSTAR GXL
591 polymerase (TaKaRa Bio) or LA Taq Hot Start Version Polymerase (TaKaRa Bio) per the
592 manufacturer's instructions. The PCR products were run on an agarose gel and bands of the
593 targeted size were cut and isolated using the QIAEX II Gel Extraction Kit (Qiagen). We
594 successfully amplified sufficient DNA for labelling for scaffolds W005, W002, and W014 to
595 confirm their order in the v9 assembly (Figure S5). Multiplex metaphase FISH and karyotyping
596 were done following the procedures previously described [76].

597 Arima-HiC data to validate the *S. mansoni* v9 assembly

598 The Arima-HiC Kit for Animal Tissues (Arima Genomics; Material Part Numbers: A510008
599 Document Part Number: A160140 v00 Release Date: November 2018) was used following the
600 manufacturer's instructions with ~100 fresh female *S. mansoni* worms as input. An Illumina
601 library was made using the Swift Biosciences Accel-NGSO 2S Plus DNA Library Kit, with the
602 modified Arima Genomics protocol. The library was sequenced on the Illumina HiSeq X Ten
603 platform resulting in high resolution with >260x coverage of the genome (Table S17). Arima-HiC
604 data was aligned to the v7 assembly using BWA [77]; version 0.7.17). The HiC contact map
605 was made with PretextMap (<https://github.com/wtsi-hpag/PretextMap>) and viewed in

606 PretextView (<https://github.com/wtsi-hpag/PretextView>) (Figure 1). Minor misassemblies and
607 placement of previously 31 unplaced scaffolds were done manually in Gap5 [75].

608 Illumina RNA-seq and PacBio IsoSeq transcriptome 609 sequencing across *S. mansoni* developmental stages

610 Illumina RNA-seq libraries were prepared with the TruSeq RNA Library Prep Kit following the
611 manufacturer's protocol. The Smart-seq2 protocol [78] was followed as described to synthesize
612 full length cDNA from 1 μ g total RNA for PacBio IsoSeq full-length transcript sequencing. cDNA
613 was amplified in 12 cycles PCR and size fractionated in SageELF electrophoresis system
614 (Sage Science). One or more cDNA size fractions were pooled for the library preparation. For
615 some samples, libraries were produced from more of the size fractions obtained from the
616 SageELF, with the aim of reducing size bias in the PacBio RSII sequencing reads (Table S3).

617 Heterozygosity in Z and W sex chromosomes and nucleotide diversity in 618 the Z chromosome

619 Genome-wide SNP calling was performed using GATK HaplotypeCaller with PCR-free Illumina
620 genomic libraries (Table S17) and 7 previously published samples (12663_1_4, 12663_2_4,
621 7164_6, 7164_7, 7307_7, 7307_8, 8040_3) [32].

622 To calculate nucleotide diversity (π), median and mean autosomal coverage was calculated for
623 all samples in the Crellen *et al.* data set [32]. Individuals with $>10x$ median and mean coverage
624 on Z and W chromosomes were retained (54 male and 61 female). Of these, the ZSR:PAR ratio
625 was calculated. Individuals with >0.70 ZSR:PAR ratio and a PAR/ZSR <1.5 were designated as
626 males and individuals with <0.70 ZSR:PAR ratio and a PAR/ZSR >1.5 were designated as
627 females. This resulted in a data set consisting of 54 males and 61 females. We used PIXY
628 (v.0.95.01) [79] to calculate π in 50 kb sliding, non-overlapping windows across each

629 chromosome separately for male and female populations for the autosomes. Nucleotide
630 diversity for the ZSR and PARs was calculated in 5 kb sliding, non-overlapping windows. We
631 then calculated the bootstrapped (95%) confidence intervals for each population median using
632 1000 bootstrap samples of genomic windows for each population using previously published
633 methods [58] (
634 https://github.com/duncanberger/PZQ_POPGEN/blob/master/Figures/figure_2.md). We
635 compared nucleotide diversity between ZSR and the PARs for male individuals testing for
636 significance using an unpaired t-test.

637 W-repeat classification and quantification

638 Dot plots were generated for each repeat array on the W chromosome contigs to ensure that a
639 representative repeat unit was selected from each visually distinct section of each repeat array.
640 This process yielded 36 unique repeat unit sequences subsequently named smw01-smw36.
641 The 36 repeat units were compared, pairwise, using blastn with a word size of 6 and dust off.
642 For each comparison with an e-value <0.01, the percentage identity and bit score was recorded
643 and plotted in a matrix plot to reveal similarities between repeat units that define repeat unit
644 families (i.e. Sm- α).

645 An attempt was made to computationally quantify the W-repeats. Using female PCR-free
646 Illumina data (sample 6520_5; Table S17), gDNA reads were mapped to 19 known single and
647 multi-copy genes (e.g. SmVAL, omega-1) and to all 36 identified W-repeat sequences. Using
648 bedtools coverage on 50 bp windows from the resulting bam file, the single-copy genes had a
649 median coverage of 67 with a range of 54 to 72 and a median of median coverages of 67.
650 SmVAL had double this (151x) and omega-1 had 10 times this (671x) as expected. Taking
651 normal coverage to be 67x, W coverage should be half that at 33.5x. From this we calculated
652 an estimated expected size for our W-repeats (Table S16).

653 Gene finding

654 Protein-coding genes

655 A new protein-coding gene set was produced for the v9 assembly from evidence-based
656 predictions from Augustus [20] with Illumina and PacBio transcriptome reads (Table S3),
657 followed by manual curation. Repeat Modeller v2.0.1 [80] and Repeat Masker v4.1.2 on
658 sensitive mode [81] were run to identify, classify, and mask repetitive elements, including low-
659 complexity sequences and interspersed repeats. The masked genome was then used for gene
660 finding with Augustus v3.2.2 [82] with the following parameters designed to predict one or more
661 splice-forms per gene: `--species=schistosoma2 --UTR=1 --alternative-from-evidence=1`. To
662 predict better gene models and alternative splicing, we used extrinsic information as evidence
663 (i.e. 'exonpart' and 'intron' hints in Augustus) based on Illumina short reads of all life stages
664 except egg (set priority = 4 in the hints file), and PacBio Iso-seq reads of three life stages (male,
665 female and schistosomula; priority = 40) (Table S3).

666 To facilitate the comparison of gene sets between assemblies, we also transferred the latest
667 gene models from v5 (based on GeneDB in July 2017) to v7 using RATT [83] with the PacBio
668 setting. The transferred gene models were then compared to those from *de novo* predictions
669 using gffcompare v0.9.9d [84], to determine consensus or novel transcripts (blastn hit of <94%
670 coverage or nucleotide identity <78% between the two assembly versions). When changes
671 occurred compared to a previous gene model, namely an amino acid sequence had changed
672 >20% in either identity or coverage as determined by blastp, or the gene was merged with
673 another gene, or split into several new genes, a new identifier (starting with Smp_3) was
674 assigned and the old Smp number(s) was kept as a previous systematic id (PSID). Otherwise,
675 the previous v5 Smp identifier was transferred to the v7 gene model. Genes that were related to
676 retrotransposons in v5, or not transferred by RATT to the v7 assembly, were not kept in the new
677 gene set. From v7 to v9, gene models were transferred using LiftOff [85]. For gene models with
678 structural changes compared to the v5 gene set, or potentially novel genes predicted by
679 Augustus in the v7 and v9 assemblies, we have carefully inspected them and curated them in
680 Web Apollo [86] (Tables S5, S6).

681 For functional annotation, blastp v2.7.0 against SwissProt was used to predict product
682 information, and InterproScan v5.25 [87]) to predict product protein domains and Gene
683 Ontology terms. For some genes their product information was preserved from the v5 gene set
684 (taken from GeneDB) if the evidence code was not “Inferred from Electronic Annotation”.

685 Coverage of UTRs in the genome sequence was calculated as following: first we extract the 5’-
686 and 3’- UTR annotations from the gff file, adding up the total UTR length for each transcript, and
687 then for each gene, we took the transcript with longest UTR as a representative. Finally, all
688 UTRs were summed up for calculating the coverage. Other feature statistics were calculated
689 using Eval v2.2.8 [88].

690 To recover possible additional novel genes from Boroni *et al* [89], the CDS/transcript sequences
691 were obtained directly from the authors and aligned to the v9 gene set using blast, where genes
692 with hits were considered as existing. For those without hits to current gene models, their
693 sequences were aligned to the whole genome using blastn and PROmer [90]. Genes with hits
694 to multiple scaffolds were discarded. For genes hitting to the same scaffold the overlapping hit
695 regions were merged using “bedtools merge” and set as “exon” in a gff. All possible models
696 were manually inspected in Apollo using the same RNA-seq tracks as in the publication. We
697 found evidence for 8 of the 759 putative novel genes reported by Boroni *et al.* [89]) (Table S20).

698 We initially assessed genome completeness using BUSCO v3.0.2 [23]. Although only 85.8%
699 complete eukaryota orthologs were found in the genome sequence (using “--mode genome”;
700 Table S7), representation is expected to be considerably less than 100% in platyhelminths due
701 to their phylogenetic distance from other species in the BUSCO databases [22]. It is known that
702 BUSCO applied to genomic sequences underestimates the completeness of assemblies due to
703 the difficulty of detecting complete genes in the assembly [91] providing further explanation for
704 missing orthologs. As an alternative, we tested the completeness of our predicted gene models
705 using BUSCO (“--mode proteins”) and recovered 95.3% complete eukaryota orthologs.

706 Transfer RNAs (tRNAs)

707 tRNAscan v.1.3.1 [92], was used to identify transfer RNAs (tRNAs) in the *S. mansoni* v9
708 assembly. The algorithm was run with default parameters except for "--forceow --cove".

709 Long intergenic non-coding RNAs (lincRNAs)

710 In order to locate long intergenic non-coding RNAs in v9 of the *S. mansoni* genome assembly,
711 we used RATT [83] to migrate previously generated annotation [93] from v5 to v9. To this end,
712 we downloaded the published annotation as a GFF file, transformed it to EMBL file (as required
713 by RATT) and proceeded to migrate the annotations using the "PacBio" setting of RATT. From
714 a total of 7,029 lincRNAs annotated in v5, 6,876 transfers were made (6,874 unique, two
715 duplications) and 273 lincRNAs were not transferred.

716 Spliced-leader RNAs (SL RNAs)

717 Using RNA-seq data (Table S3), we have located SL (spliced leader) sequences in 6,497
718 genes (Table S8) or 66.3% of all annotated genes in the primary assembly. SL sequences were
719 identified using the canonical *S. mansoni* SL sequence
720 AACCGTCACGGTTTTACTCTTGTGATTTGTTGCATG (Genbank M34074.1 [94]) and a custom
721 in-house spliced leader detection script [95]
722 ([https://github.com/stephenrdoyle/hcontortus_genome/blob/5543173b7ee83b903d976931813d](https://github.com/stephenrdoyle/hcontortus_genome/blob/5543173b7ee83b903d976931813d85f96f7a6e13/03_code/hcontortus_genome.section5_workbook.md)
723 [85f96f7a6e13/03_code/hcontortus_genome.section5_workbook.md](https://github.com/stephenrdoyle/hcontortus_genome/blob/5543173b7ee83b903d976931813d85f96f7a6e13/03_code/hcontortus_genome.section5_workbook.md)). The script first trims a
724 predefined SL sequence from the 5' end of RNA-seq reads allowing for a minimum length
725 match with an allowed error rate of 10% using Cutadapt [96]. The trimmed sequences are
726 extracted, sorted, and counted, making a sequence logo. The trimmed reads are mapped to the
727 genome using HiSat2 [97] and a BAM file of the mapped trimmed reads is generated for
728 visualisation. A BED file is also made of the splice site coordinates along with a WebLogo [98]
729 of 20 bp surrounding the splice site. Finally, the script determines the coverage of splice sites

730 with transcript starts, (200 bp upstream and 30 bp downstream of the annotated start codon)
731 and internal CDSs, accounting for both misannotated and internal splice variants.

732 Following published methods [30], we looked for alternative SL sequences using a custom
733 python script to identify reads that (a) aligned to annotated genes, or within 500 bp upstream,
734 and (b) were soft-clipped by more than 5 bp at the 5' end relative to the annotated gene. Soft-
735 clipped sequences were clustered using CD-HIT-EST v4.7 [99] and only one prominent cluster
736 was identified. Thus, the *S. mansoni* SL sequence appears to be highly conserved within the
737 genome, and there is only one sequence with the abundance of the known SL sequence,
738 occurring in around 10% of the randomly chosen RNA reads.

739 Gene clusters and gene density in the *S. mansoni* genome

740 To explore whether there are particular gene functions overrepresented on some
741 chromosomes, we searched for genomically adjacent genes (≥ 3) with the same Pfam
742 annotations. To investigate whether gene families that had been incorrectly collapsed in the v5
743 assembly and are now expanded in the v9 assembly, this analysis was performed for both v5
744 and v9 using Pfam annotations from InterproScan (see "Protein coding genes" section above).
745 For clusters with at least 5 genes, the start coordinates of the first and last genes as well as the
746 number of genes were indicated (Table S2).

747 IPSE and omega-1 were found to be multi-copy genes clustered in two tandem repeat regions.
748 In order to compare how many bases of curated IPSE and omega-1 genes could be mapped to
749 the v5 and v7 assemblies, we ran Exonerate with a max intron size of 1,500 bp for both IPSE
750 and omega. The IPSE gene Smp_112110 was used in Exonerate, but for omega-1, the mRNA
751 sequence was used because the omega-1 gene has a long and complex gene structure. GFF
752 files were produced of mapped features for IPSE and omega-1 which served to illustrate how
753 many copies of these genes could be annotated.

754 The IPSE v9 sequence is 199,167 bp with the equivalent v5 sequence is 86,067 bp. The gap in
755 v9 is approximately 29 kb larger than the total of the gaps in v5 in this region. There are
756 approximately 84 additional kilobases in v9 in this region mostly due to expansion of repeat
757 sequence to give a closer representation of reality (Figure S2). Likewise, the omega-1 v9
758 sequence is 155,103 bp and the v5 sequence is 105,726 bp. There is a 29,982 bp increase due
759 to a large gap in v9, leaving 19,395 bp of additional sequence mainly due to expansion of the
760 repeat array.

761 Gene expression across different *S. mansoni* life stages and sexes

762 To explore gene transcript levels across different life stages and between males and females,
763 previously published RNA-seq data [40,41] was used. Briefly, reads were mapped to *S.*
764 *mansoni* v9 genome using STAR v2.4.2a [100]. Counts per gene and TPMs were summarised
765 with StringTie v2.1.4 [101]. Mean TPM values were calculated for samples of the same life
766 stage and sex and log-transformed. For gametologue expression, only unique mapping reads
767 were used for quantification.

768 In comparing gene expression of gametologues on WSR and ZSR regions, the ACT genome
769 browser [102] was used with PROmer version 3.07 [103] to show sequence similarity. A
770 transposon inserted into the Smp_318710 pseudogenes was annotated based on PROmer
771 sequence similarity to other transposons on ZSR. For Figure 7, bm_1, bm_2, bm_3 male
772 libraries and bf_1, bf_2, bf_3 female libraries were used [104]. For Figure S7b, bf_1 was used.

773 Identification of centromeres and telomeres

774 A 123 bp tandem repeat motif was identified in *S. mansoni* by Melters *et al* [26] due to its high
775 abundance (~1% of the genomic reads), relative to all other tandem repeats in the genome. The
776 original consensus was derived from multiple chromosomes and an almost identical motif is
777 present in chromosomes 1-3, 5-7, and W (Table S11). On both chromosome 4 and Z, single

778 candidate tandem repeats were identified with broadly similar repeat lengths and sequences to
779 previously described consensus motif [26].

780 We examined repeats in Gap5 [75], taking only the portion of the repeat with the centromere
781 tandem repeat motif. Centromere size estimates (Table S11) were based on Illumina genomic
782 sequencing from female clonally-derived cercariae (sample ERS039722 from Table S17)
783 mapped to 1 representative repeat unit of each of the 8 centromere repeats. As a control, reads
784 were also mapped to the 1st 121 bp of the genomic sequence covered by 12 known single copy
785 genes. These 12 genes gave us a median coverage of 15x. From this we were able to
786 extrapolate sizes for each of the 8 centromeric repeats which totalled 2.25 Mb.

787 A MAFFT/Jalview alignment was created from all centromere motif sequences [105] and a
788 neighbor-joining tree was constructed using the ETE Toolkit Phylogenetic tree viewer [106]
789 (Table S11). Centromere motif sequence similarity was assessed using the alignment tool
790 PRSS with the Smith-Waterman algorithm (https://embnet.vital-it.ch/software/PRSS_form.html
791 [107,108]).

792 Hirai and LoVerde [109] determined the sequence motif of schistosome telomeres (CCCTAA
793 repeat) through FISH detection. In African schistosomes, the telomeric repeat sequence can be
794 found in the heterochromatin and centromere of the W chromosome. Because it is theorized
795 that *Schistosoma* originated in Asia (see review [110]), the African schistosomes experienced
796 more gene shuffling than the Asian schistosomes, accounting for the presence of telomeric
797 repeats outside the ends of the chromosomes [111].

798 Abbreviations

799 PAR: pseudoautosomal region

800 WSR: W-specific region

801 ZSR: Z-specific region

802 BUSCO: Benchmarking Universal Single Copy Orthologs

803 Mb: megabase

804 Kb: kilobase

805 bp: base pair

806 aa: amino acid

807 tRNA: transfer RNA

808 lincRNA: long intergenic non-coding

809 SL: spliced leader

810 SLTS: spliced leader trans-splicing

811 NOR: nucleolar organizer region; rDNA

812 Declarations

813 Ethics approval

814 To propagate the life cycle of the *Schistosoma mansoni* NMRI strain (Puerto Rican) and obtain
815 different developmental stages of the parasite, BALB/c mice and susceptible BB02 strain
816 *Biomphalaria glabrata* snails are routinely infected with parasites at the Wellcome Sanger
817 Institute (WSI). The mouse infections were conducted under Home Office Project Licence No.
818 80/2596 and No. P77E8A062, and all protocols were presented and approved by the Animal
819 Welfare and Ethical Review Body (AWERB) of the WSI. The AWERB is constituted as required
820 by the UK Animals (Scientific Procedures) Act 1986 Amendment Regulations 2012. With the
821 exception of sporocysts and miracidia, all life cycle stages were collected at the WSI.

822 *Schistosoma mansoni* SmbRE strain sporocysts dissected from infected BB02 *B. glabrata*
823 snails were collected at The University of Perpignan laboratory which has permission A 66040
824 from both the French Ministère de l'agriculture et de la pêche and the French Ministère de
825 l'Education Nationale de la Recherche et de la Technologie for experiments on animals and
826 certificate for animal experimentation (authorization 007083, decree 87-848 and 2012201-0008)
827 for the experimenters. Housing, breeding and animal care follow the national ethical
828 requirements.

829 *Schistosoma mansoni* NMRI strain miracidia were collected at Justus-Liebig-University Giessen
830 Institute for Parasitology. Animal experiments were approved by the Regional Council
831 (Regierungspräsidium), Giessen, Germany (V54-19 c 20/15 c GI 18/10), which are in
832 accordance with the European Convention for the Protection of Vertebrate Animals used for
833 experimental and other scientific purposes (ETS No 123; revised Appendix A).

834 Consent for publication

835 Not applicable

836 Availability of data and materials

837 The primary genome assembly generated and analyzed during this study are available on the
838 European Nucleotide Archive (ENA) website under project accession PRJEB13987. Additional
839 assembled haplotypes, haplotype annotations, and primary assembly annotations can be found
840 in permanent links at WormBase ParaSite under BioProject PRJEA36577 and at Zenodo
841 DOI:10.5281/zenodo.5149023. All other data generated or analyzed during this study are
842 included in this published article and its supplementary information files.

843

844 Competing interests

845 The authors declare that they have no competing interests.

846 Funding

847 This work was supported by the Wellcome Trust grants 098051 and 206194. For the purpose of
848 Open Access, the authors have applied a CC BY public copyright licence to any Author
849 Accepted Manuscript version arising from this submission.

850 Authors' contributions

851 MB designed research, which was coordinated by NH; SKB and GR maintained the parasite life
852 cycle and generated parasite material, SKB, DB, and GS prepared genomic DNA, RNA and
853 transcriptome sequencing libraries; BF, FY, and SKB performed FISH experiments; SKB, AT,
854 ZL, SD, DB, FR, AJR, UB analyzed data; SKB drafted the complete manuscript, with sections of
855 text contributed by AT, AJR and ZL. All authors read and approved the final manuscript.

856 Acknowledgements

857 The *Schistosoma mansoni* genome project is funded by the Wellcome Trust through their core
858 support of the Wellcome Trust Sanger Institute (grant 098051 and 206194). We thank Simon
859 Claire and his team for technical assistance with the life cycle maintenance and collection of
860 parasite material. We thank Tom Huckvale, Hayley Bennet, and Arporn Wangwiwatsin for
861 technical support in generating RNA-seq and gDNA libraries. Thank you to Christoph Puethe
862 for assisting in the ENA submission. A special thank you to Karl Hoffman and Josephine Ford-
863 Thomas for supplying additional infected snails used for metaphase FISH, Paul Brindley and
864 Victoria Mann for clonal worms, and Christoph Grunau and Benjamin Gourbal for providing *in*
865 *vivo* sporocysts for RNA-seq.

866 Figure and table legends

867 **Figure 1: Ideograms of the *S. mansoni* chromosomes with HiC plots showing end-to-end**
868 **chromosomal resolution.** (a) Representative ZZ (male) and ZW (female) *S. mansoni*
869 metaphase spreads, karyotypes, and ideograms. The yellow arrowheads point to the nucleolar
870 organizer region (NOR; rDNA). Grey regions are euchromatic DNA, black are constitutive
871 heterochromatin (C-band) regions, blue is confirmed telomeric sequence, and light blue bands
872 are confirmed sub-telomeric sequence. (b) HiC visualization plots from genome version 5 (left)
873 and version 9 (right) with the yellow arrowhead pointing to the NOR in chromosome 3.

874 **Table 1: Genome-wide statistics for the *S. mansoni* haploid v9 assembly compared to the**
875 **previous v5 assembly.** The v9 assembly size has grown considerably with the addition of 26.9
876 Mb. The number of gaps present between versions was reduced by 96%, the majority of which
877 are now only present in the collapsed repeat regions of the W chromosome. The chromosomes
878 are assembled into 9 scaffolds (autosomes 1-7, W, and Z). Characterization of SLTS (spliced
879 leader trans-splicing) in the transcripts has increased our previous estimates of only 7% of
880 transcripts being trans-spliced to over 72% in the current assembly. *Completely new,
881 previously partial, or previously unannotated.

882 **Figure 2: Improvements in the Z-specific region of the Z chromosome between the**
883 **previous v5 *S.mansoni* genome assembly and current v9 assembly.** Assemblies were
884 compared using PROmer and visualized in ACT. The v5 assembly contained a partially
885 resolved Z chromosome with misassemblies and between the Z-specific region (ZSR) and
886 pseudoautosomal regions (PARs). Corrected inversions from v5 to v9 are shown in lighter blue.
887 Coverage of mapped sequencing reads from female-only sequencing libraries highlight the ZSR
888 as a region with approximately half the depth of coverage as pseudoautosomal regions.

889 **Figure 3: Z-specific regions of African and Asian *Schistosoma* spp. evolved differentially**
890 **from an ancestral region that coincides with a likely fusion between chromosomes.** (a)

891 Evolutionary strata are defined through \log_2 genome coverage on the x-axis of one-to-one
892 orthologs in four schistosomes and the hermaphroditic platyhelminth *Echinostoma caproni*. The
893 African-specific stratum in dark purple defines Z-specific region 1 (ZSR1) of *S. mansoni* where
894 approximately half coverage is seen in the African schistosomes *S. mansoni*, *S. rodhaini*, and
895 *S. haematobium*. The Asian-specific stratum in green has reduced coverage specific only to *S.*
896 *japonicum* with two possible inversions shown in green brackets. The ancestral *Schistosoma*
897 stratum represents the schistosome orthologs ancestrally isolated to the Z sex chromosome
898 between all schistosome species. (b) Tapeworm orthologs and chromosome synteny blocks
899 show evidence of the fusion in the schistosome lineage between chromosomes 3 and 5 of the
900 tapeworm *Echinococcus multilocularis*. Figure 3b adapted from Olson *et al* [30].

901 Figure 4: **Median nucleotide diversity (π ; pi) across the protein-coding genes of the**
902 **autosomes, PARs, and Z-specific regions using published genome variation data [32].**

903 Median nucleotide diversity (π ; pi) was calculated separately for males (left) and females (right)
904 in 50 kb windows (a,b) or 5 kb windows (c-f) across all protein-coding genes. Pi is shown for the
905 autosomes (a,b), PARs and ZSRs (c,d) and combined autosomal regions and ZSRs (e,f).

906 Figure 5: **Detailed, annotated idiograms of the Z and W sex chromosomes.** (a) The true
907 size of the W chromosome is approximately 14% larger than Z which can be accounted for in
908 the large expansion of repeats in the WSR. All but 36 genes have been lost on the WSR with 5
909 of those being pseudogenes and 2 present in triplicate and duplicate. Chevrons mark the
910 approximate location of 3 euchromatin bands in the WSR. (b) The assembled size of the WSR
911 is ~6 Mb, less than its true size of ~46 Mb because of 36 collapsed repeats. (c) C-banding
912 shows the alternating AT- and GC-rich DNA repeats present in the WSR.

913 Figure 6: **Illumina RNA-seq expression of the W and Z gametologues in adult paired and**
914 **naive male and female *S. mansoni* worms.** Unique mapping of RNA-seq to the gametologues
915 reveals relatively similar expression of the Z gametologues between males and females for
916 most gametologues. As expected, the W gametologues show expression limited to the female

917 samples. Lines connect gametologue pairs between Z and W. In two cases, the W
918 gametologue exists in triplicate or duplicate (see W gametologues Smp_317860, Smp_317870,
919 Smp_348710 and Smp_318680, Smp_318860).

920 **Figure 7: A comparison of U2AF 65 kDa subunit gametologues on the Z and W**
921 **chromosomes.** The gametologues of the large, 65 kDa subunit of U2AF (Z: Smp_019690; W:
922 Smp_348790) are shown on ZSR (top) and WSR (bottom). Predicted transcript sequences in
923 yellow. Sequence similarity was determined using PROmer and shows that the N-terminal
924 region of the coding sequence (blue) is more diverse. The black arrow head highlights the
925 position of a likely sequencing error on WSR which causes a frameshift, but which has been
926 corrected in the gene model. Unnormalised coverage of RNA-seq reads is shown for female
927 (bf_1, bf_2, bf_3) and male samples (bm_1, bm_2, bm_3). This highlights male expression on
928 only the ZSR, with lower female coverage on ZSR and WSR as expected. Numbers above
929 gene models indicate position on the contigs, numbers above RNA-seq coverage indicate
930 maximum read depth.

931 **Figure 8: Hypothetical illustration of the schistosome Z and W sex chromosome**
932 **evolution.** A chromosomal fusion between two ancestral schistosome autosomes occurred
933 near the ZSR stratum boundary (see Figure 3) creating a new set of autosomes. Followed by,
934 or in conjunction with, this fusion event, a male antagonistic and/or female advantageous locus
935 was isolated on the pre-sex chromosomes (see Figure 6; potentially pre-mRNA splicing factor
936 U2AF). The need to isolate the phenotypic effects of the gene(s) in this locus on the pre-W
937 chromosome required recombination suppression (see Figure 4). Isolation of additional loci with
938 sex-specific effects and elimination and/or pseudogenization of non-sex-specific coding loci is
939 evidenced in Fig 5. Following initial recombination suppression, extensive
940 heterochromatinization of W ensured long-term recombination suppression between W and Z
941 sex-specific regions and resulted in the huge expansion of repeats in the W-specific region
942 (Figure 5; Table S16)

943 Additional Files

944 Additional file 1: **Supplementary Tables S1 to S20**

945 Supplementary Figures Titles and Legends

946 Figure S1: **Array of spliced-leader RNA genes on chromosome 6 of the *S. mansoni***

947 **genome.** On chromosome six, a 62.6 kb locus exists containing 41 full-length spliced leader

948 RNA genes (top track). An additional 109 partial gene sequences that contain the spliced leader

949 exon sequence only exist in the same array (bottom track).

950

951 Figure S2: **Resolving the repetitive IPSE and omega-1 loci.** Genes in the (a) IPSE loci and

952 (b) Omega-1 locus shown in v9 through gene model annotations (top tracks) and genomic

953 coverage mapping (bottom tracks) with yellow boxes to connect gene annotations to genomic

954 coverage. The annotations show the v9 gene models, some of which coincide with elevated

955 read coverage. The histogram in the coverage plots show depth of read coverage and

956 compared with the flanking regions, the depth is elevated in the IPSE and omega-1 loci

957 suggesting these gene arrays are smaller in this assembly than their true size.

958 Figure S3: **Gene changes from genome v5 to v9 of *S. mansoni*.** There have been a total of

959 3,610 gene changes represented by 810 new, 867 deleted, 344 merged, 189 multiple copies,

960 190 split, and 1,210 structurally changed. The bar graph shows totals of different protein-coding

961 gene changes in the primary assembly (i.e. no gene fragments, haplotypes, or pseudogenes).

962

963 Figure S4: **Alignment of the centromeric repeat sequences relatedness between all *S.***

964 ***mansoni* chromosomes.** MAFFT/Jalview alignment of a single centromeric repeat unit from

965 each chromosome shows high similarity between chromosomes 1-3, 5-7, and W.

966 Chromosomes 1-3, 5-7, and W are 93.1-98.5% identical to a 123bp centromeric repeat

967 proposed by Melters *et al* [26]. The centromeric repeats for chromosomes 4 and Z are diverged
968 from the other chromosomes.

969 **Figure S5: Validation of the assembly and placement of W-specific scaffolds using**
970 **metaphase FISH.** Twenty-two W-specific scaffolds existed after computational and manual
971 assembly. Scaffold W007 contained the junction from PAR1 into the WSR and scaffold W016
972 spanned the WSR into PAR2. The centromeric repeat for the W chromosome was in scaffold
973 W002 (7.65-7.75 Mb) with the orientation of this contig inferred from alignment of centromere
974 sequence in this scaffold. The remaining 8 scaffolds with gametologues (purple) and 11
975 scaffolds without gametologues (black), whose positions and orientations could not be
976 determined using sequence data alone, were placed using metaphase FISH.

977

978 **Figure S6: Measurements of Z and W chromosomes from 6 female metaphase cells.** The
979 W chromosome is approximately 14.7% larger than the Z chromosome based on
980 measurements taken of the chromosomes from the metaphase figures shown. Measurements
981 were taken using the measurement tool in Inkscape. This figure is consistent with previously
982 published measurements from 22 female metaphase cells [33].

983 **Figure S7: Comparisons of ancestral region gametologues between ZSR and WSR.** (a)
984 The Z gametologue Smp_158310 is clearly expressed in males (red RNA-seq coverage) and
985 females (blue RNA-seq coverage), but the W gametologue Smp_318710 is not. Furthermore,
986 the gene model is incomplete on WSR and there is a transposon inserted within the gene (red
987 bar), resulting in a pseudogene. The genes are inverted between ZSR and WSR, indicated by
988 the overlapping sequence similarity bars. (b) The genome sequence for the WSR gametologue
989 of U2AF 65kDa (Smp_348790) subunit contains a single base insertion, suggesting a possible
990 frameshift mutation. However, RNA-seq reads show that this is a sequencing error and the
991 corrected gene model based on this data results in an N-terminal amino acid sequence more
992 similar to, although still somewhat divergent from, the Z gametologue (Smp_019690).

993 References

- 994 1. Toor J, Alsallaq R, Truscott JE, Turner HC, Werkman M, Gurarie D, et al. Are We on Our Way to Achieving the
995 2020 Goals for Schistosomiasis Morbidity Control Using Current World Health Organization Guidelines? *Clin Infect*
996 *Dis.* 2018;66:S245–52. Available from: <http://dx.doi.org/10.1093/cid/ciy001>
- 997 2. Colley DG, Bustinduy AL, Secor WE, King CH. Human schistosomiasis. *Lancet.* 2014;383:2253–64. Available
998 from: [http://dx.doi.org/10.1016/S0140-6736\(13\)61949-2](http://dx.doi.org/10.1016/S0140-6736(13)61949-2)
- 999 3. Loker ES, Brant SV. Diversification, dioecy and dimorphism in schistosomes. *Trends Parasitol.* 2006;22:521–8.
1000 Available from: <http://dx.doi.org/10.1016/j.pt.2006.09.001>
- 1001 4. Platt TR, Brooks DR. Evolution of the schistosomes (Digenea: Schistosomatoidea): the origin of dioecy and
1002 colonization of the venous system. *J Parasitol.* 1997;83:1035–44. Available from:
1003 <https://www.ncbi.nlm.nih.gov/pubmed/9406775>
- 1004 5. Tomaszewicz M, Medvedev P, Makova KD. Y and W Chromosome Assemblies: Approaches and Discoveries.
1005 *Trends in Genetics.* 2017. p. 266–82. Available from: <http://dx.doi.org/10.1016/j.tig.2017.01.008>
- 1006 6. Xue L, Gao Y, Wu M, Tian T, Fan H, Huang Y, et al. Telomere-to-telomere assembly of a fish Y chromosome
1007 reveals the origin of a young sex chromosome pair. *Genome Biol.* 2021;22:203. Available from:
1008 <http://dx.doi.org/10.1186/s13059-021-02430-y>
- 1009 7. Mahajan S, Wei KH-C, Nalley MJ, Gibilisco L, Bachtrog D. De novo assembly of a young Drosophila Y
1010 chromosome using single-molecule sequencing and chromatin conformation capture. *PLoS Biol.* 2018;16:e2006348.
1011 Available from: <http://dx.doi.org/10.1371/journal.pbio.2006348>
- 1012 8. Bellott DW, Skaletsky H, Cho T-J, Brown L, Locke D, Chen N, et al. Avian W and mammalian Y chromosomes
1013 convergently retained dosage-sensitive regulators. *Nat Genet.* 2017;49:387–94. Available from:
1014 <http://dx.doi.org/10.1038/ng.3778>
- 1015 9. Skaletsky H, Kuroda-Kawaguchi T, Minx PJ, Cordum HS, Hillier L, Brown LG, et al. The male-specific region of the
1016 human Y chromosome is a mosaic of discrete sequence classes. *Nature.* 2003;423:825–37. Available from:
1017 <http://dx.doi.org/10.1038/nature01722>
- 1018 10. Hirai H, Spotila LD, LoVerde PT. Schistosoma mansoni: chromosomal localization of DNA repeat elements by in
1019 situ hybridization using biotinylated DNA probes. *Exp Parasitol.* 1989;69:175–88. Available from:
1020 <https://www.ncbi.nlm.nih.gov/pubmed/2753121>
- 1021 11. Berriman M, Haas BJ, LoVerde PT, Wilson RA, Dillon GP, Cerqueira GC, et al. The genome of the blood fluke
1022 Schistosoma mansoni. *Nature.* 2009;460:352–8. Available from: <http://dx.doi.org/10.1038/nature08160>
- 1023 12. Protasio AV, Tsai IJ, Babbage A, Nichol S, Hunt M, Aslett MA, et al. A systematically improved high quality
1024 genome and transcriptome of the human blood fluke Schistosoma mansoni. *PLoS Negl Trop Dis.* 2012;6:e1455.
1025 Available from: <http://dx.doi.org/10.1371/journal.pntd.0001455>
- 1026 13. Abdulla M-H, Lim K-C, McKerrow JH, Caffrey CR. Proteomic identification of IPSE/alpha-1 as a major
1027 hepatotoxin secreted by Schistosoma mansoni eggs. *PLoS Negl Trop Dis.* 2011;5:e1368. Available from:
1028 <http://dx.doi.org/10.1371/journal.pntd.0001368>
- 1029 14. Everts B, Perona-Wright G, Smits HH, Hokke CH, van der Ham AJ, Fitzsimmons CM, et al. Omega-1, a
1030 glycoprotein secreted by Schistosoma mansoni eggs, drives Th2 responses. *J Exp Med.* 2009;206:1673–80.
1031 Available from: <http://dx.doi.org/10.1084/jem.20082460>
- 1032 15. Costain AH, MacDonald AS, Smits HH. Schistosome Egg Migration: Mechanisms, Pathogenesis and Host
1033 Immune Responses. *Front Immunol.* 2018;9:3042. Available from: <http://dx.doi.org/10.3389/fimmu.2018.03042>
- 1034 16. Hagen J, Young ND, Every AL, Pagel CN, Schnoeller C, Scheerlinck J-PY, et al. Omega-1 knockdown in
1035 Schistosoma mansoni eggs by lentivirus transduction reduces granuloma size in vivo. *Nat Commun.* 2014;5:5375.
1036 Available from: <http://dx.doi.org/10.1038/ncomms6375>
- 1037 17. Ranasinghe SL, Fischer K, Gobert GN, McManus DP. Functional expression of a novel Kunitz type protease
1038 inhibitor from the human blood fluke Schistosoma mansoni. *Parasit Vectors.* 2015;8:408. Available from:
1039 <http://dx.doi.org/10.1186/s13071-015-1022-z>
- 1040 18. Ingram JR, Rafi SB, Alegria Eroy-Reveles A, Ray M, Lambeth L, Hsieh I, et al. Investigation of the Proteolytic
1041 Functions of an Expanded Cercarial Elastase Gene Family in Schistosoma mansoni. *PLoS Neglected Tropical*
1042 *Diseases.* 2012. p. e1589. Available from: <http://dx.doi.org/10.1371/journal.pntd.0001589>

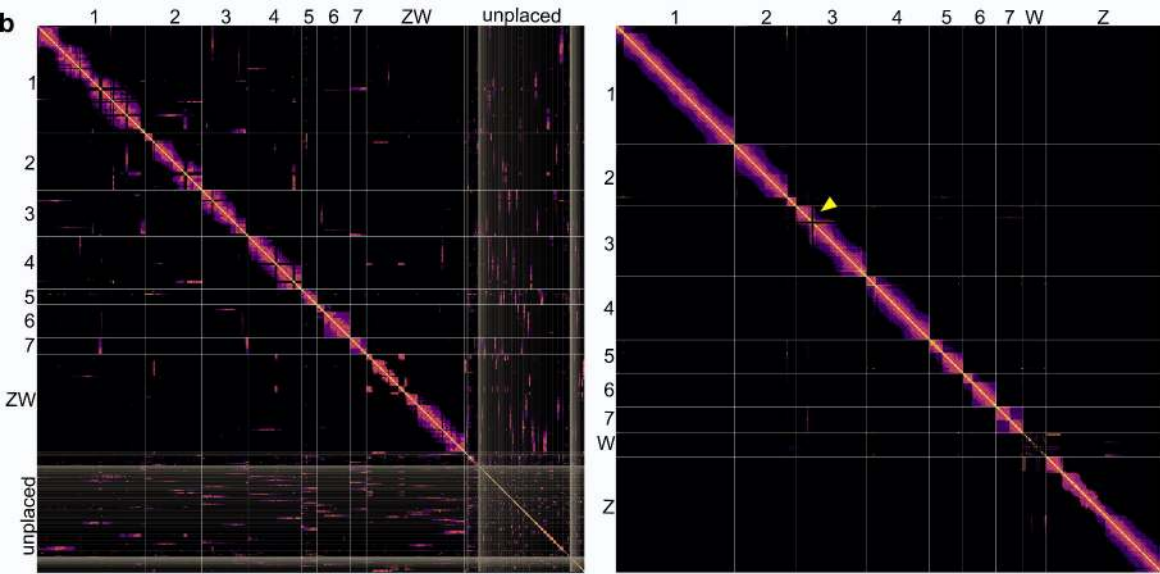
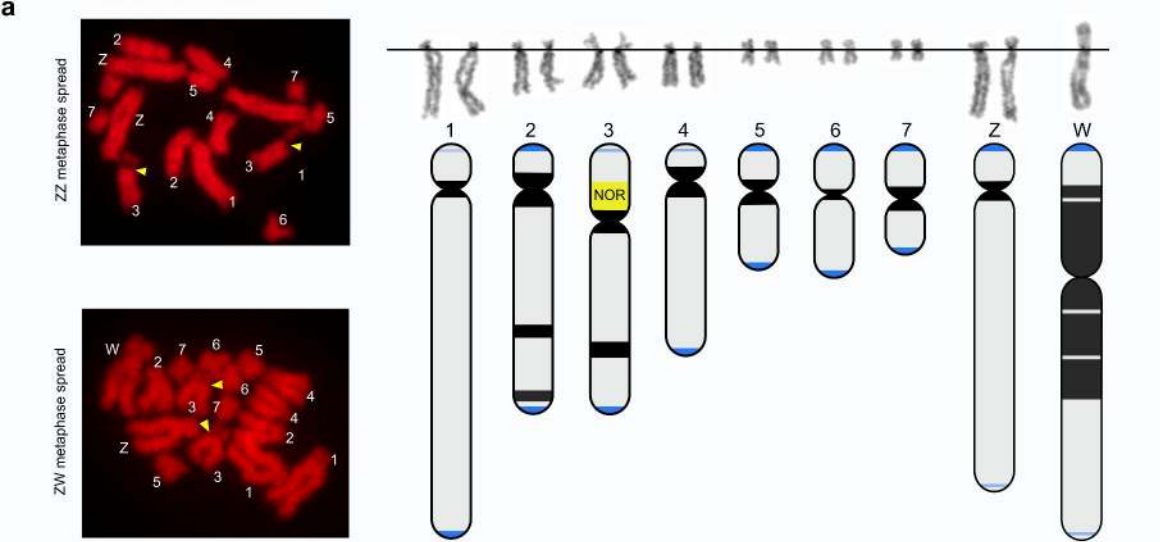
- 1043 19. Buddenborg SK, Kamel B, Hanelt B, Bu L, Zhang S-M, Mkoji GM, et al. The in vivo transcriptome of *Schistosoma*
1044 *mansoni* in two prominent vector species, *Biomphalaria pfeifferi* and *B. glabrata*. 2019. Available from:
1045 <https://journals.plos.org/plosntds/article?id=10.1371/journal.pntd.0007013>
- 1046 20. Stanke M, Morgenstern B. AUGUSTUS: a web server for gene prediction in eukaryotes that allows user-defined
1047 constraints. *Nucleic Acids Res.* 2005;33:W465–7. Available from: <http://dx.doi.org/10.1093/nar/gki458>
- 1048 21. Tsai IJ, Zarowiecki M, Holroyd N, Garcarrubio A, Sánchez-Flores A, Brooks KL, et al. The genomes of four
1049 tapeworm species reveal adaptations to parasitism. *Nature.* 2013;496:57–63. Available from:
1050 <http://dx.doi.org/10.1038/nature12031>
- 1051 22. Olson PD, Tracey A, Baillie A, James K, Doyle SR. Complete representation of a tapeworm genome reveals
1052 chromosomes capped by centromeres, necessitating a dual role in segregation and protection. *bioRxiv.* biorxiv.org;
1053 2020; Available from: <https://www.biorxiv.org/content/10.1101/2020.04.08.031872v1.abstract>
- 1054 23. Waterhouse RM, Seppey M, Simão FA, Manni M, Ioannidis P, Klioutchnikov G, et al. BUSCO Applications from
1055 Quality Assessments to Gene Prediction and Phylogenomics. *Mol Biol Evol.* Oxford Academic; 2017 [cited 2020 Nov
1056 3];35:543–8. Available from: <https://academic.oup.com/mbe/article-pdf/35/3/543/24367705/msx319.pdf>
- 1057 24. Allen MA, Hillier LW, Waterston RH, Blumenthal T. A global analysis of *C. elegans* trans-splicing. *Genome Res.*
1058 2011;21:255–64. Available from: <http://dx.doi.org/10.1101/gr.113811.110>
- 1059 25. Short RB, Grossman AI. Conventional Giemsa and C-Banded Karyotypes of *Schistosoma mansoni* and *S.*
1060 *rodhaini*. *The Journal of Parasitology.* 1981. p. 661. Available from: <http://dx.doi.org/10.2307/3280440>
- 1061 26. Melters DP, Bradnam KR, Young HA, Telis N, May MR, Ruby JG, et al. Comparative analysis of tandem repeats
1062 from hundreds of species reveals unique insights into centromere evolution. *Genome Biol.* 2013;14:R10. Available
1063 from: <http://dx.doi.org/10.1186/gb-2013-14-1-r10>
- 1064 27. Picard MAL, Cosseau C, Ferré S, Quack T, Grevelding CG, Couté Y, et al. Evolution of gene dosage on the Z-
1065 chromosome of schistosome parasites. *Elife.* 2018;7. Available from: <http://dx.doi.org/10.7554/eLife.35684>
- 1066 28. Lepesant JMJ, Cosseau C, Boissier J, Freitag M, Portela J, Climent D, et al. Chromatin structural changes
1067 around satellite repeats on the female sex chromosome in *Schistosoma mansoni* and their possible role in sex
1068 chromosome emergence. *Genome Biol.* 2012;13:R14. Available from: <http://dx.doi.org/10.1186/gb-2012-13-2-r14>
- 1069 29. Hirai H, Hirai Y, LoVerde PT. Evolution of sex chromosomes ZW of *Schistosoma mansoni* inferred from
1070 chromosome paint and BAC mapping analyses. *Parasitol Int.* 2012;61:684–9. Available from:
1071 <http://dx.doi.org/10.1016/j.parint.2012.07.007>
- 1072 30. Olson PD, Tracey A, Baillie A, James K, Doyle SR, Buddenborg SK, et al. Complete representation of a
1073 tapeworm genome reveals chromosomes capped by centromeres, necessitating a dual role in segregation and
1074 protection. *BMC Biol.* 2020;18:165. Available from: <http://dx.doi.org/10.1186/s12915-020-00899-w>
- 1075 31. Wilson Sayres MA. Genetic Diversity on the Sex Chromosomes. *Genome Biol Evol.* 2018;10:1064–78. Available
1076 from: <http://dx.doi.org/10.1093/gbe/evy039>
- 1077 32. Crellen T, Allan F, David S, Durrant C, Huckvale T, Holroyd N, et al. Whole genome resequencing of the human
1078 parasite *Schistosoma mansoni* reveals population history and effects of selection. *Sci Rep.* 2016;6:20954. Available
1079 from: <http://dx.doi.org/10.1038/srep20954>
- 1080 33. Hirai H, Spotila LD, LoVerde PT. *Schistosoma mansoni*: chromosomal localization of DNA repeat elements by in
1081 situ hybridization using biotinylated DNA probes. *Exp Parasitol.* 1989;69:175–88. Available from:
1082 <https://www.ncbi.nlm.nih.gov/pubmed/2753121>
- 1083 34. Ebbert MTW, Jensen TD, Jansen-West K, Sens JP, Reddy JS, Ridge PG, et al. Systematic analysis of dark and
1084 camouflaged genes reveals disease-relevant genes hiding in plain sight. *Genome Biol.* BioMed Central; 2019 [cited
1085 2020 Oct 9];20:1–23. Available from: <https://genomebiology.biomedcentral.com/articles/10.1186/s13059-019-1707-2>
- 1086 35. Poptsova MS, Il'icheva IA, Nechipurenko DY, Panchenko LA, Khodikov MV, Oparina NY, et al. Non-random DNA
1087 fragmentation in next-generation sequencing. *Sci Rep.* Nature Publishing Group; 2014 [cited 2020 Oct 9];4:1–6.
1088 Available from: <https://www.nature.com/articles/srep04532>
- 1089 36. Drew AC, Brindley PJ. Female-specific sequences isolated from *Schistosoma mansoni* by representational
1090 difference analysis. *Mol Biochem Parasitol.* 1995;71:173–81. Available from: [http://dx.doi.org/10.1016/0166-6851\(95\)00048-6](http://dx.doi.org/10.1016/0166-6851(95)00048-6)
- 1092 37. Spotila LD, Hirai H, Rekosh DM, Lo Verde PT. A retroposon-like short repetitive DNA element in the genome of
1093 the human blood fluke, *Schistosoma mansoni*. *Chromosoma.* 1989;97:421–8. Available from:

- 1094 <http://dx.doi.org/10.1007/BF00295025>
- 1095 38. Spotila LD, LoVerde PT, Rekosh DM. Analysis of two repeated DNA sequences of *Schistosoma mansoni*. UCLA
1096 symposium on Molecular and Cellular Biology, 6ol. 1987. p. 159–68.
- 1097 39. Madeira F, Park YM, Lee J, Buso N, Gur T, Madhusoodanan N, et al. The EMBL-EBI search and sequence
1098 analysis tools APIs in 2019. *Nucleic Acids Res.* 2019;47:W636–41. Available from:
1099 <http://dx.doi.org/10.1093/nar/gkz268>
- 1100 40. Lu Z, Sessler F, Holroyd N, Hahnel S, Quack T, Berriman M, et al. A gene expression atlas of adult *Schistosoma*
1101 *mansoni* and their gonads. *Sci Data.* 2017;4:170118. Available from: <http://dx.doi.org/10.1038/sdata.2017.118>
- 1102 41. Picard MAL, Boissier J, Roquis D, Grunau C, Allienne J-F, Duval D, et al. Sex-Biased Transcriptome of
1103 *Schistosoma mansoni*: Host-Parasite Interaction, Genetic Determinants and Epigenetic Regulators Are Associated
1104 with Sexual Differentiation. *PLoS Negl Trop Dis.* 2016;10:e0004930. Available from:
1105 <http://dx.doi.org/10.1371/journal.pntd.0004930>
- 1106 42. Rawlinson KA, Reid AJ, Lu Z, Driguez P, Wawer A. Daily rhythms in the transcriptomes of the human parasite
1107 *Schistosoma mansoni*. *bioRxiv.* biorxiv.org; 2021; Available from:
1108 <https://www.biorxiv.org/content/10.1101/2021.04.21.440693v2.abstract>
- 1109 43. Everts B, Perona-Wright G, Smits HH, Hokke CH, van der Ham AJ, Fitzsimmons CM, et al. Omega-1, a
1110 glycoprotein secreted by *Schistosoma mansoni* eggs, drives Th2 responses. *J Exp Med.* 2009;206:1673–80.
1111 Available from: <http://dx.doi.org/10.1084/jem.20082460>
- 1112 44. Schwartz C, Fallon PG. *Schistosoma* “Eggs-lting” the Host: Granuloma Formation and Egg Excretion. *Front*
1113 *Immunol.* 2018;9:2492. Available from: <http://dx.doi.org/10.3389/fimmu.2018.02492>
- 1114 45. Foster JM, Grote A, Mattick J, Tracey A, Tsai Y-C, Chung M, et al. Sex chromosome evolution in parasitic
1115 nematodes of humans. *Nature Communications.* 2020. Available from: <http://dx.doi.org/10.1038/s41467-020-15654-6>
- 1116 46. Sahara K, Yoshido A, Traut W. Sex chromosome evolution in moths and butterflies. *Chromosome Res.*
1117 2012;20:83–94. Available from: <http://dx.doi.org/10.1007/s10577-011-9262-z>
- 1118 47. Singh RK, Singh D, Yadava A, Srivastava AK. Molecular fossils “pseudogenes” as functional signature in
1119 biological system. *Genes Genomics.* 2020;42:619–30. Available from: <https://doi.org/10.1007/s13258-020-00935-7>
- 1120 48. Picard MAL, Vicoso B, Bertrand S, Escriva H. Diversity of Modes of Reproduction and Sex Determination
1121 Systems in Invertebrates, and the Putative Contribution of Genetic Conflict. *Genes.* 2021. p. 1136. Available from:
1122 <http://dx.doi.org/10.3390/genes12081136>
- 1123 49. Elkrewi M, Moldovan MA, Picard MAL, Vicoso B. Schistosome W-linked genes inform temporal dynamics of sex
1124 chromosome evolution and suggest candidate for sex determination. *Mol Biol Evol.* 2021; Available from:
1125 <http://dx.doi.org/10.1093/molbev/msab178>
- 1126 50. Krämer A. The structure and function of proteins involved in mammalian pre-mRNA splicing. *Annu Rev Biochem.*
1127 1996;65:367–409. Available from: <http://dx.doi.org/10.1146/annurev.bi.65.070196.002055>
- 1128 51. Rudner DZ, Kanaar R, Breger KS, Rio DC. Mutations in the small subunit of the *Drosophila* U2AF splicing factor
1129 cause lethality and developmental defects. *Proc Natl Acad Sci U S A.* 1996;93:10333–7. Available from:
1130 <http://dx.doi.org/10.1073/pnas.93.19.10333>
- 1131 52. Bashaw GJ, Baker BS. The *msl-2* dosage compensation gene of *Drosophila* encodes a putative DNA-binding
1132 protein whose expression is sex specifically regulated by *Sex-lethal*. *Development.* 1995;121:3245–58. Available
1133 from: <https://www.ncbi.nlm.nih.gov/pubmed/7588059>
- 1134 53. Kelley RL, Solovyeva I, Lyman LM, Richman R, Solovyev V, Kuroda MI. Expression of *msl-2* causes assembly of
1135 dosage compensation regulators on the X chromosomes and female lethality in *Drosophila*. *Cell.* 1995;81:867–77.
1136 Available from: [http://dx.doi.org/10.1016/0092-8674\(95\)90007-1](http://dx.doi.org/10.1016/0092-8674(95)90007-1)
- 1137 54. Bachtrog D, Mank JE, Peichel CL, Kirkpatrick M, Otto SP, Ashman T-L, et al. Sex determination: why so many
1138 ways of doing it? *PLoS Biol.* 2014;12:e1001899. Available from: <http://dx.doi.org/10.1371/journal.pbio.1001899>
- 1139 55. Dean R, Mank JE. The role of sex chromosomes in sexual dimorphism: discordance between molecular and
1140 phenotypic data. *Journal of Evolutionary Biology.* 2014. p. 1443–53. Available from:
1141 <http://dx.doi.org/10.1111/jeb.12345>
- 1142 56. Graves JAM. Sex chromosome specialization and degeneration in mammals. *Cell.* 2006;124:901–14. Available
1143 from: <http://dx.doi.org/10.1016/j.cell.2006.02.024>

- 1144 57. Charlesworth D, Charlesworth B, Marais G. Steps in the evolution of heteromorphic sex chromosomes. *Heredity*.
1145 2005;95:118–28. Available from: <http://dx.doi.org/10.1038/sj.hdy.6800697>
- 1146 58. Berger D, Crellen T, Lambert PHL, Allan F, Tracey A, Noonan JD, et al. Data release: Whole-genome
1147 sequencing of *Schistosoma mansoni* reveals extensive diversity with limited selection despite mass drug
1148 administration. 2021. Available from: <https://zenodo.org/record/5045162>
- 1149 59. Le Clec'h W, Chevalier FD, Mattos ACA, Strickland A, Diaz R, McDew-White M, et al. Genetic analysis of
1150 praziquantel resistance in schistosome parasites implicates a Transient Receptor Potential channel. *bioRxiv*. 2021
1151 [cited 2021 Aug 10]. p. 2021.06.09.447779. Available from:
1152 <https://www.biorxiv.org/content/10.1101/2021.06.09.447779v1.abstract>
- 1153 60. Picard MAL, Vicoso B, Roquis D, Bulla I, Augusto RC, Arancibia N, et al. Dosage Compensation throughout the
1154 *Schistosoma mansoni* Lifecycle: Specific Chromatin Landscape of the Z Chromosome. *Genome Biol Evol*.
1155 2019;11:1909–22. Available from: <http://dx.doi.org/10.1093/gbe/evz133>
- 1156 61. Augusto R de C, de Carvalho Augusto R, Cosseau C, Grunau C. Histone Methylome of the Human Parasite
1157 *Schistosoma Mansoni*. *RNA Technologies*. 2019. p. 607–24. Available from: http://dx.doi.org/10.1007/978-3-030-14792-1_24
1158
- 1159 62. Roquis D, Taudt A, Geyer KK, Padalino G, Hoffmann KF, Holroyd N, et al. Histone methylation changes are
1160 required for life cycle progression in the human parasite *Schistosoma mansoni*. *PLoS Pathog*. 2018;14:e1007066.
1161 Available from: <http://dx.doi.org/10.1371/journal.ppat.1007066>
- 1162 63. Mann VH, Morales ME, Rinaldi G, Brindley PJ. Culture for genetic manipulation of developmental stages of
1163 *Schistosoma mansoni*. *Parasitology*. 2010;137:451–62. Available from:
1164 <http://dx.doi.org/10.1017/S0031182009991211>
- 1165 64. Lewis F. *Schistosomiasis*. *Curr Protoc Immunol*. 2001;Chapter 19:Unit 19.1. Available from:
1166 <http://dx.doi.org/10.1002/0471142735.im1901s28>
- 1167 65. Grevelding CG, Kampkötter A, Kunz W. *Schistosoma mansoni*: sexing cercariae by PCR without DNA extraction.
1168 *Exp Parasitol*. 1997;85:99–100. Available from: <http://dx.doi.org/10.1006/expr.1996.4129>
- 1169 66. Wangwiwatsin A, Protasio AV, Wilson S, Owusu C. Transcriptome of the parasitic flatworm *Schistosoma*
1170 *mansoni* during intra-mammalian development. *bioRxiv*. [www.biorxiv.org; 2019](https://www.biorxiv.org/10.1101/757633v1); Available from:
1171 <https://www.biorxiv.org/content/10.1101/757633v1.abstract>
- 1172 67. Park N, Shirley L, Gu Y, Keane TM, Swerdlow H, Quail MA. An improved approach to mate-paired library
1173 preparation for Illumina sequencing. *Methods in Next Generation Sequencing*. 2013;1. Available from:
1174 <http://access.portico.org/stable?au=pgj2kqzq4j1>
- 1175 68. Kozarewa I, Ning Z, Quail MA, Sanders MJ, Berriman M, Turner DJ. Amplification-free Illumina sequencing-
1176 library preparation facilitates improved mapping and assembly of (G+C)-biased genomes. *Nat Methods*. 2009;6:291–
1177 5. Available from: <http://dx.doi.org/10.1038/nmeth.1311>
- 1178 69. Kuk FK, Tyler RS, Rustad N, Harker LA, Tye-Murray N. Alternating current at the eardrum for tinnitus reduction. *J*
1179 *Speech Hear Res*. 1989;32:393–400. Available from: <http://dx.doi.org/10.1044/jshr.3202.393>
- 1180 70. Criscione CD, Valentim CLL, Hirai H, LoVerde PT, Anderson TJC. Genomic linkage map of the human blood
1181 fluke *Schistosoma mansoni*. *Genome Biol*. 2009;10:R71. Available from: <http://dx.doi.org/10.1186/gb-2009-10-6-r71>
- 1182 71. Tsai IJ, Otto TD, Berriman M. Improving draft assemblies by iterative mapping and assembly of short reads to
1183 eliminate gaps. *Genome Biol*. 2010;11:R41. Available from: <http://dx.doi.org/10.1186/gb-2010-11-4-r41>
- 1184 72. Nadalin F, Vezzi F, Policriti A. GapFiller: a de novo assembly approach to fill the gap within paired reads. *BMC*
1185 *Bioinformatics*. 2012;13 Suppl 14:S8. Available from: <http://dx.doi.org/10.1186/1471-2105-13-S14-S8>
- 1186 73. Bankevich A, Nurk S, Antipov D, Gurevich AA, Dvorkin M, Kulikov AS, et al. SPAdes: a new genome assembly
1187 algorithm and its applications to single-cell sequencing. *J Comput Biol*. 2012;19:455–77. Available from:
1188 <http://dx.doi.org/10.1089/cmb.2012.0021>
- 1189 74. Koren S, Walenz BP, Berlin K, Miller JR, Bergman NH, Phillippy AM. Canu: scalable and accurate long-read
1190 assembly via adaptive k-mer weighting and repeat separation. *Genome Res*. 2017;27:722–36. Available from:
1191 <http://dx.doi.org/10.1101/gr.215087.116>
- 1192 75. Bonfield JK, Whitwham A. Gap5--editing the billion fragment sequence assembly. *Bioinformatics*. 2010;26:1699–
1193 703. Available from: <http://dx.doi.org/10.1093/bioinformatics/btq268>

- 1194 76. Algady W, Louzada S, Carpenter D, Brajer P, Färner A, Rooth I, et al. The Malaria-Protective Human
1195 Glycophorin Structural Variant DUP4 Shows Somatic Mosaicism and Association with Hemoglobin Levels. *Am J*
1196 *Hum Genet.* 2018;103:769–76. Available from: <http://dx.doi.org/10.1016/j.ajhg.2018.10.008>
- 1197 77. Li H, Durbin R. Fast and accurate short read alignment with Burrows-Wheeler transform. *Bioinformatics.*
1198 2009;25:1754–60. Available from: <http://dx.doi.org/10.1093/bioinformatics/btp324>
- 1199 78. Picelli S, Faridani OR, Björklund AK, Winberg G, Sagasser S, Sandberg R. Full-length RNA-seq from single cells
1200 using Smart-seq2. *Nat Protoc.* 2014;9:171–81. Available from: <http://dx.doi.org/10.1038/nprot.2014.006>
- 1201 79. Korunes KL, Samuk K. pixy: Unbiased estimation of nucleotide diversity and divergence in the presence of
1202 missing data. *bioRxiv.* [biorxiv.org; 2020](https://doi.org/10.1101/2020.06.27.175091v1); Available from:
1203 <https://www.biorxiv.org/content/10.1101/2020.06.27.175091v1.abstract>
- 1204 80. Flynn JM, Hubley R, Goubert C, Rosen J, Clark AG, Feschotte C, et al. RepeatModeler2 for automated genomic
1205 discovery of transposable element families. *Proc Natl Acad Sci U S A.* 2020;117:9451–7. Available from:
1206 <http://dx.doi.org/10.1073/pnas.1921046117>
- 1207 81. Smit, AFA, Hubley, R & Green, P. RepeatMasker Open-4.0. RepeatMasker. 2013-2015. Available from:
1208 <<http://www.repeatmasker.org>>
- 1209 82. König S, Romoth LW, Gerischer L, Stanke M. Simultaneous gene finding in multiple genomes. *Bioinformatics.*
1210 2016;32:3388–95. Available from: <http://dx.doi.org/10.1093/bioinformatics/btw494>
- 1211 83. Otto TD, Dillon GP, Degraeve WS, Berriman M. RATT: Rapid Annotation Transfer Tool. *Nucleic Acids Res.*
1212 2011;39:e57. Available from: <http://dx.doi.org/10.1093/nar/gkq1268>
- 1213 84. Perteua G. GffCompare. 2018.
- 1214 85. Shumate A, Salzberg SL. Liftoff: accurate mapping of gene annotations. *Bioinformatics.* 2021. Available from:
1215 <http://dx.doi.org/10.1093/bioinformatics/btaa1016>
- 1216 86. Lee E, Helt GA, Reese JT, Munoz-Torres MC, Childers CP, Buels RM, et al. Web Apollo: a web-based genomic
1217 annotation editing platform. *Genome Biol.* 2013;14:R93. Available from: <http://dx.doi.org/10.1186/gb-2013-14-8-r93>
- 1218 87. Jones P, Binns D, Chang H-Y, Fraser M, Li W, McAnulla C, et al. InterProScan 5: genome-scale protein function
1219 classification. *Bioinformatics.* 2014;30:1236–40. Available from: <http://dx.doi.org/10.1093/bioinformatics/btu031>
- 1220 88. Keibler E, Brent MR. Eval: a software package for analysis of genome annotations. *BMC Bioinformatics.*
1221 2003;4:50. Available from: <http://dx.doi.org/10.1186/1471-2105-4-50>
- 1222 89. Boroni M, Sammeth M, Gava SG, Jorge NAN, Macedo AM, Machado CR, et al. Landscape of the spliced leader
1223 trans-splicing mechanism in *Schistosoma mansoni*. *Sci Rep.* 2018;8:3877. Available from:
1224 <http://dx.doi.org/10.1038/s41598-018-22093-3>
- 1225 90. Delcher AL, Phillippy A, Carlton J, Salzberg SL. Fast algorithms for large-scale genome alignment and
1226 comparison. *Nucleic Acids Res.* 2002;30:2478–83. Available from: <http://dx.doi.org/10.1093/nar/30.11.2478>
- 1227 91. Jebb D, Huang Z, Pippel M, Hughes GM, Lavrichenko K, Devanna P, et al. Six reference-quality genomes reveal
1228 evolution of bat adaptations. *Nature.* 2020;583:578–84. Available from: <http://dx.doi.org/10.1038/s41586-020-2486-3>
- 1229 92. Lowe TM, Chan PP. tRNAscan-SE On-line: integrating search and context for analysis of transfer RNA genes.
1230 *Nucleic Acids Res.* 2016;44:W54–7. Available from: <http://dx.doi.org/10.1093/nar/gkw413>
- 1231 93. Vasconcelos EJR, daSilva LF, Pires DS, Lavezzo GM, Pereira ASA, Amaral MS, et al. The *Schistosoma mansoni*
1232 genome encodes thousands of long non-coding RNAs predicted to be functional at different parasite life-cycle
1233 stages. *Sci Rep.* 2017;7:10508. Available from: <http://dx.doi.org/10.1038/s41598-017-10853-6>
- 1234 94. Rajkovic A, Davis RE, Simonsen JN, Rottman FM. A spliced leader is present on a subset of mRNAs from the
1235 human parasite *Schistosoma mansoni*. *Proc Natl Acad Sci U S A.* 1990;87:8879–83. Available from:
1236 <http://dx.doi.org/10.1073/pnas.87.22.8879>
- 1237 95. Doyle SR, Tracey A, Laing R, Holroyd N, Bartley D, Bazant W, et al. Genomic and transcriptomic variation
1238 defines the chromosome-scale assembly of *Haemonchus contortus*, a model gastrointestinal worm. *Commun Biol.*
1239 2020;3:656. Available from: <http://dx.doi.org/10.1038/s42003-020-01377-3>
- 1240 96. Martin M. Cutadapt removes adapter sequences from high-throughput sequencing reads. *EMBnet.journal.* 2011
1241 [cited 2020 Apr 6];17:10–2. Available from: <http://journal.embnet.org/index.php/embnetjournal/article/view/200>
- 1242 97. Kim D, Langmead B, Salzberg SL. hisat2. *Nat Methods.* 2015; Available from:

- 1243 https://ccb.jhu.edu/software/hisat2/data/HISAT2-first_release-Sept_8_2015.pdf
- 1244 98. Crooks GE, Hon G, Chandonia J-M, Brenner SE. WebLogo: a sequence logo generator. *Genome Res.* 2004;14:1188–90. Available from: <http://dx.doi.org/10.1101/gr.849004>
- 1245
- 1246 99. Fu L, Niu B, Zhu Z, Wu S, Li W. CD-HIT: accelerated for clustering the next-generation sequencing data. *Bioinformatics.* 2012;28:3150–2. Available from: <http://dx.doi.org/10.1093/bioinformatics/bts565>
- 1247
- 1248 100. Dobin A, Davis CA, Schlesinger F, Drenkow J, Zaleski C, Jha S, et al. STAR: ultrafast universal RNA-seq aligner. *Bioinformatics.* 2013;29:15–21. Available from: <http://dx.doi.org/10.1093/bioinformatics/bts635>
- 1249
- 1250 101. Perteu M, Perteu GM, Antonescu CM, Chang T-C, Mendell JT, Salzberg SL. StringTie enables improved reconstruction of a transcriptome from RNA-seq reads. *Nat Biotechnol.* 2015;33:290–5. Available from: <http://dx.doi.org/10.1038/nbt.3122>
- 1251
- 1252
- 1253 102. Carver TJ, Rutherford KM, Berriman M, Rajandream M-A, Barrell BG, Parkhill J. ACT: the Artemis Comparison Tool. *Bioinformatics.* 2005;21:3422–3. Available from: <http://dx.doi.org/10.1093/bioinformatics/bti553>
- 1254
- 1255 103. Marçais G, Delcher AL, Phillippy AM, Coston R, Salzberg SL, Zimin A. MUMmer4: A fast and versatile genome alignment system. *PLoS Comput Biol.* 2018;14:e1005944. Available from: <http://dx.doi.org/10.1371/journal.pcbi.1005944>
- 1256
- 1257
- 1258 104. Lu Z, Sessler F, Holroyd N, Hahnel S, Quack T, Berriman M, et al. Schistosome sex matters: a deep view into gonad-specific and pairing-dependent transcriptomes reveals a complex gender interplay. *Sci Rep.* 2016;6:31150. Available from: <http://dx.doi.org/10.1038/srep31150>
- 1259
- 1260
- 1261 105. Waterhouse AM, Procter JB, Martin DMA, Clamp M, Barton GJ. Jalview Version 2—a multiple sequence alignment editor and analysis workbench. *Bioinformatics.* 2009;25:1189–91. Available from: <http://dx.doi.org/10.1093/bioinformatics/btp033>
- 1262
- 1263
- 1264 106. Huerta-Cepas J, Serra F, Bork P. ETE 3: Reconstruction, Analysis, and Visualization of Phylogenomic Data. *Mol Biol Evol.* 2016;33:1635–8. Available from: <http://dx.doi.org/10.1093/molbev/msw046>
- 1265
- 1266 107. Pearson WR, Lipman DJ. Improved tools for biological sequence comparison. *Proc Natl Acad Sci U S A.* 1988;85:2444–8. Available from: <http://dx.doi.org/10.1073/pnas.85.8.2444>
- 1267
- 1268 108. Karlin S, Altschul SF. Methods for assessing the statistical significance of molecular sequence features by using general scoring schemes. *Proceedings of the National Academy of Sciences.* 1990. p. 2264–8. Available from: <http://dx.doi.org/10.1073/pnas.87.6.2264>
- 1269
- 1270
- 1271 109. Hirai H, LoVerde PT. Identification of the telomeres on *Schistosoma mansoni* chromosomes by FISH. *J Parasitol.* 1996;82:511–2. Available from: <https://www.ncbi.nlm.nih.gov/pubmed/8636864>
- 1272
- 1273 110. Lawton SP, Hirai H, Ironside JE, Johnston DA, Rollinson D. Genomes and geography: genomic insights into the evolution and phylogeography of the genus *Schistosoma*. *Parasit Vectors.* 2011;4:131. Available from: <http://dx.doi.org/10.1186/1756-3305-4-131>
- 1274
- 1275
- 1276 111. Hirai H. Chromosomal differentiation of schistosomes: what is the message? *Front Genet. Frontiers;* 2014;5:301. Available from: <https://www.frontiersin.org/articles/10.3389/fgene.2014.00301/full>
- 1277



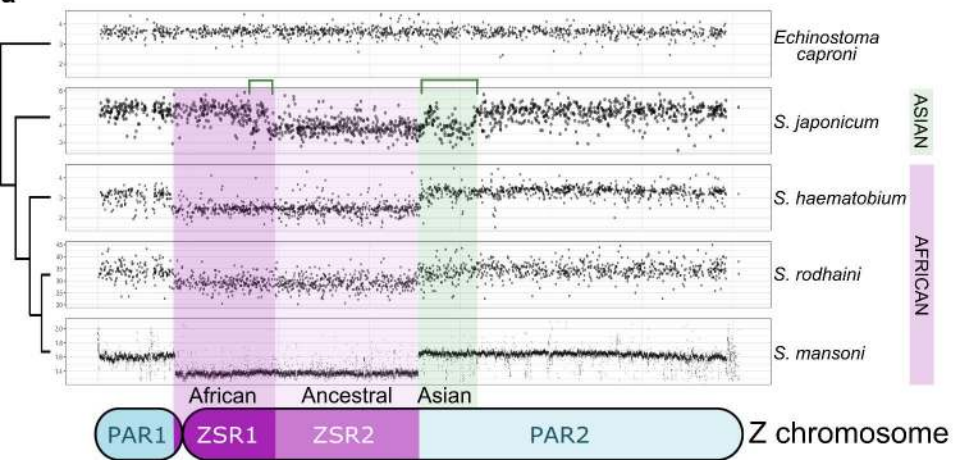
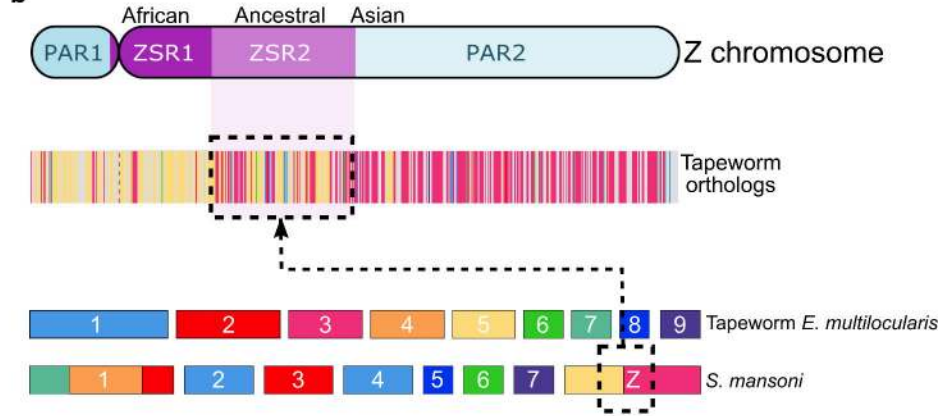
Z chromosome

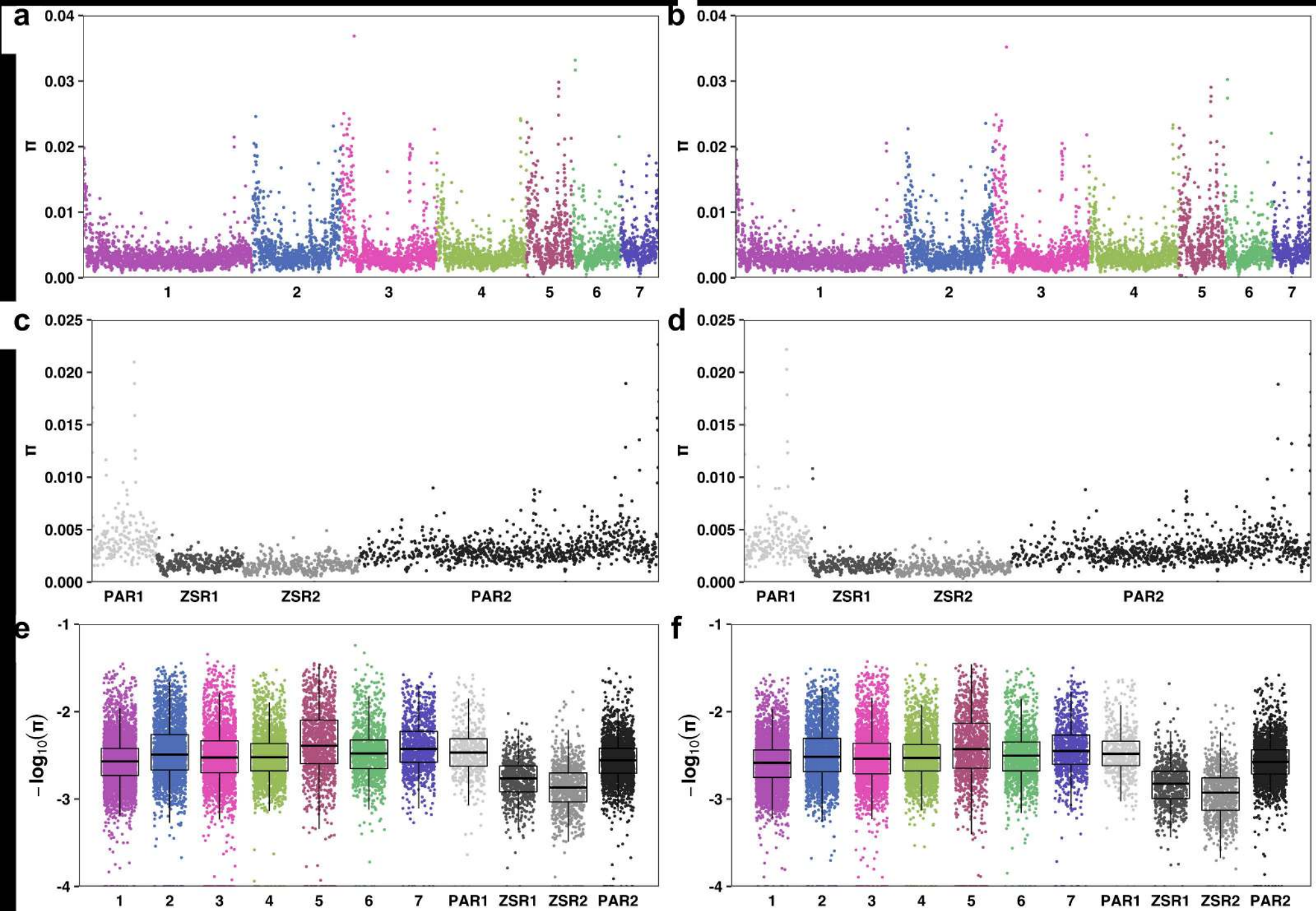


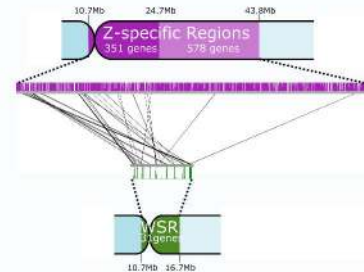
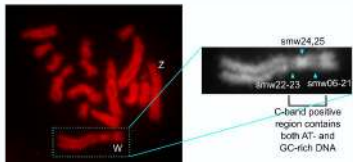
PAR1

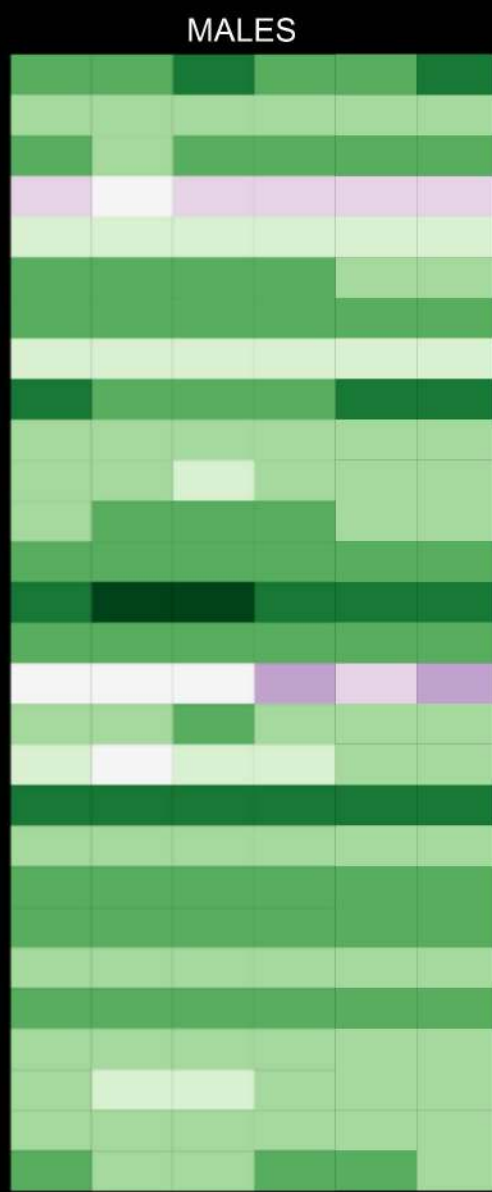
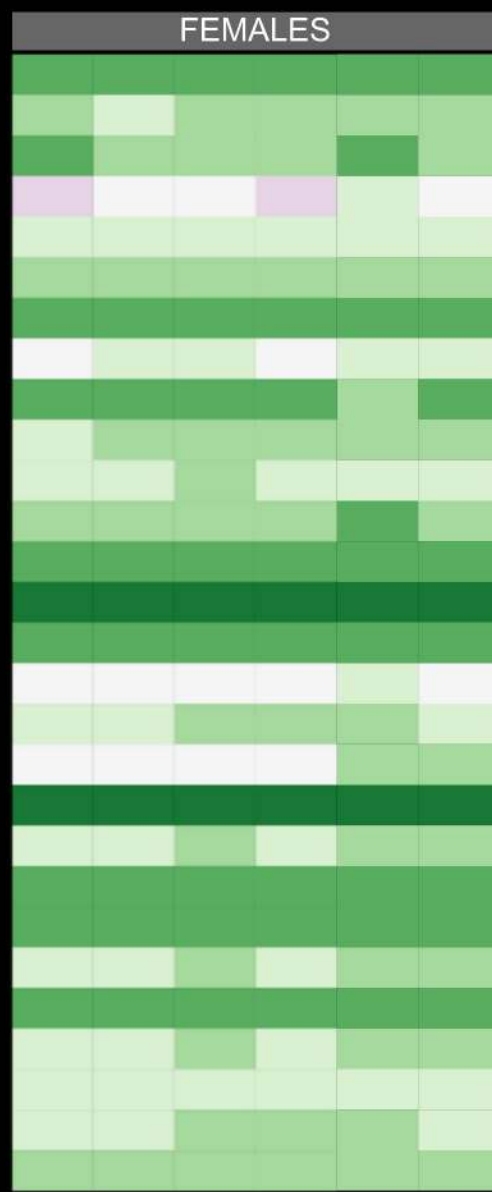
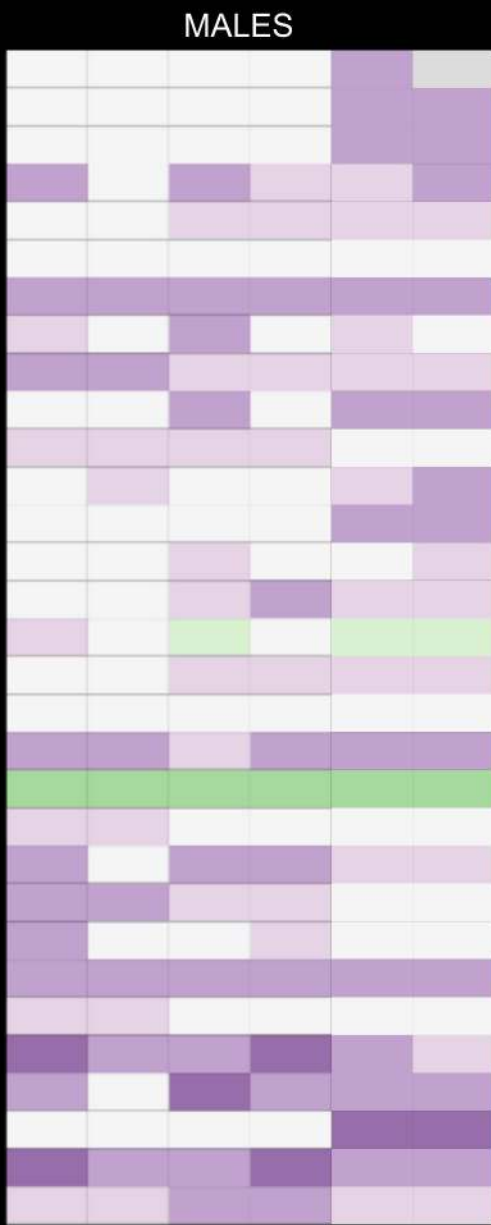
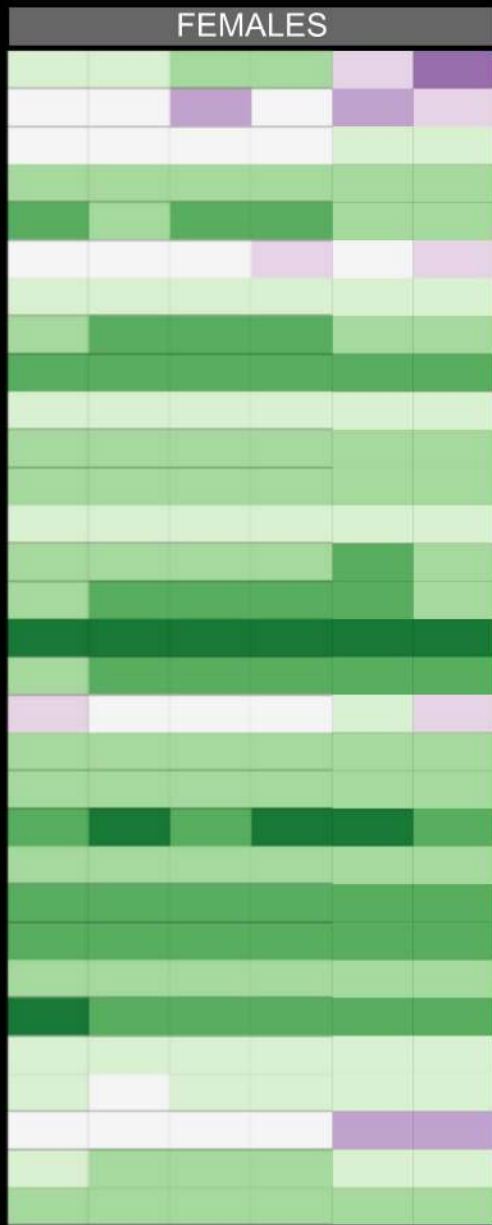
Z-specific Region

PAR2

a**b**



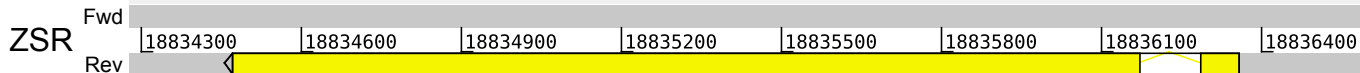
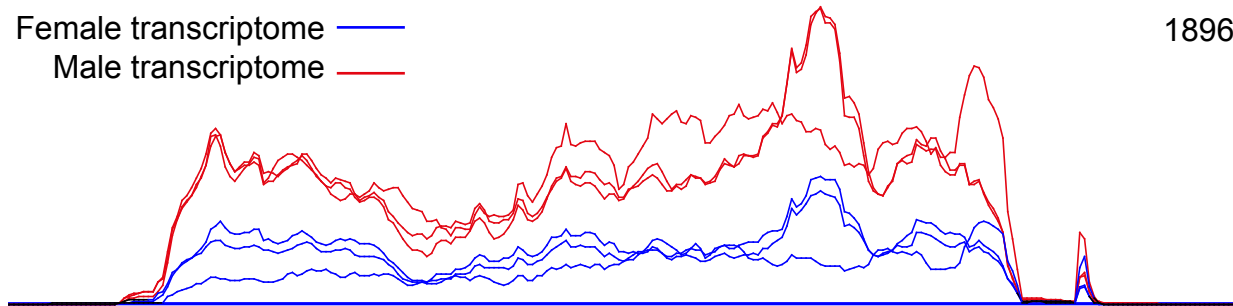
a True Z and W chromosomes**b** Assembled ZSR and WSR**c**



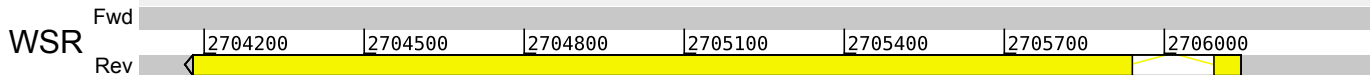
Female transcriptome

Male transcriptome

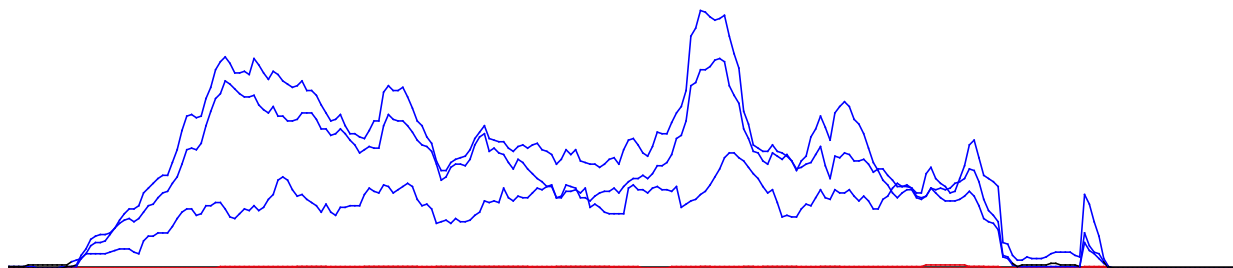
1896

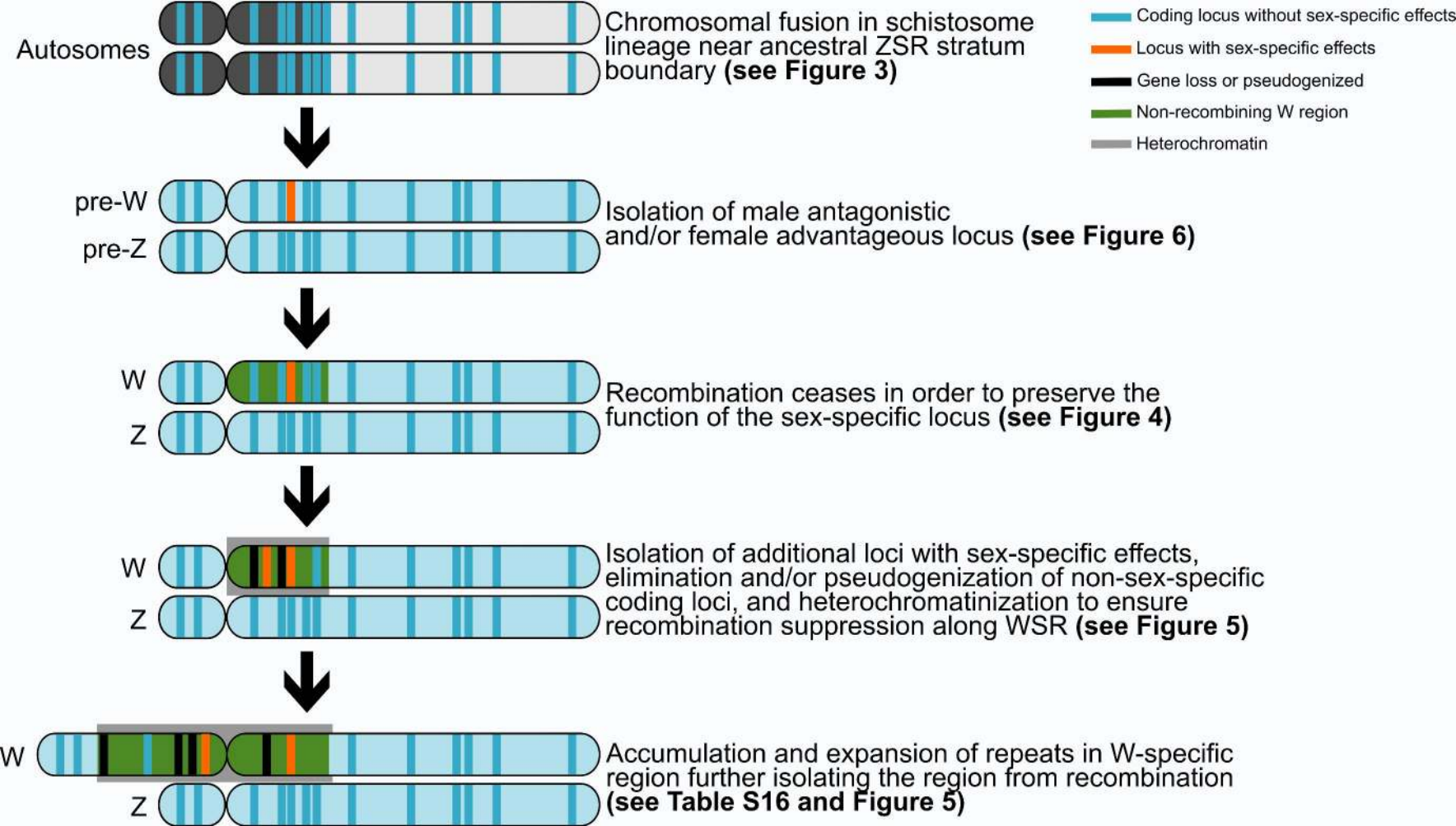


Sequence
similarity



506





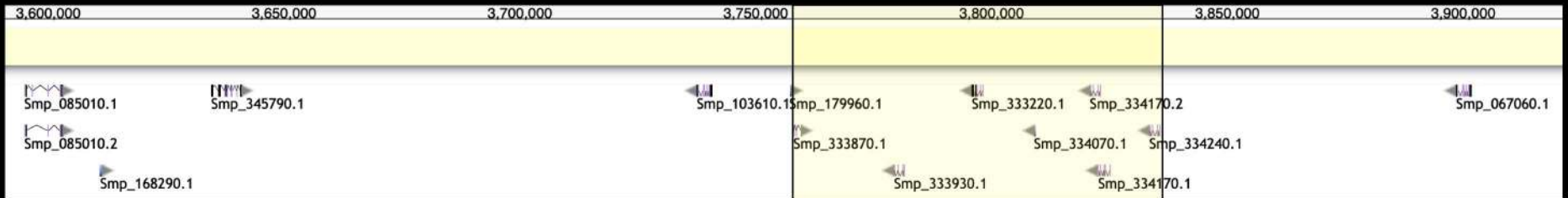
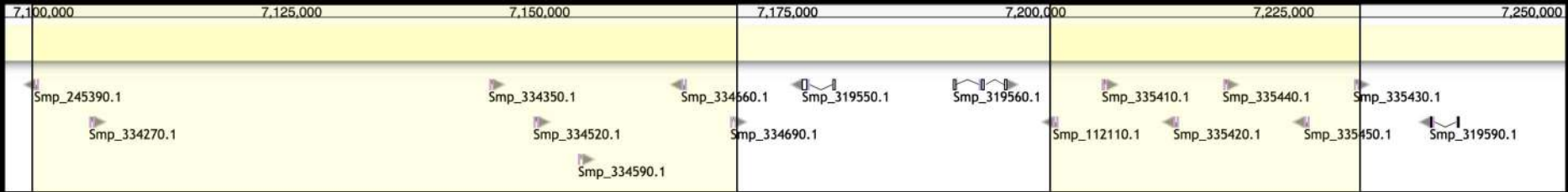
6,825,000 6,850,000 6,875,000 6,900,000 6,925,000 6,950,000

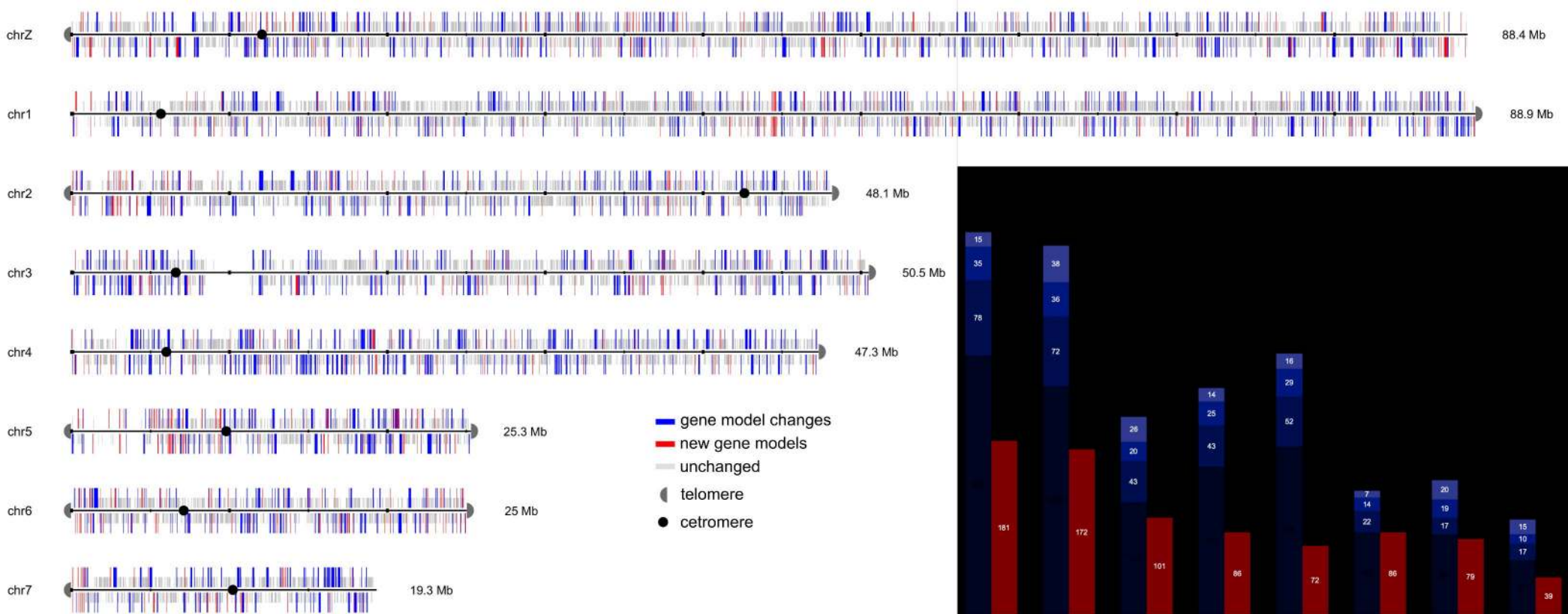
Full-length SL genes

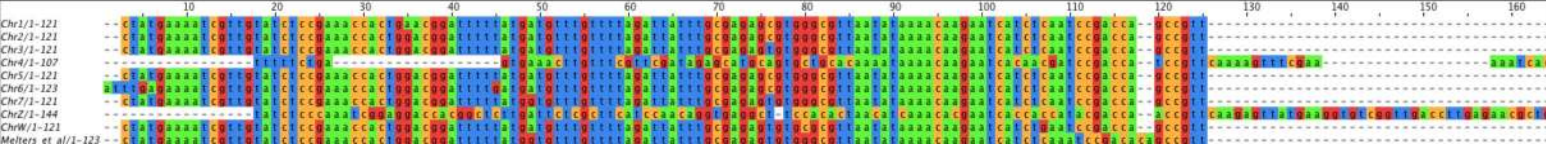


SL exons











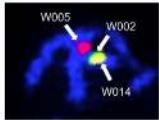
W007

W002

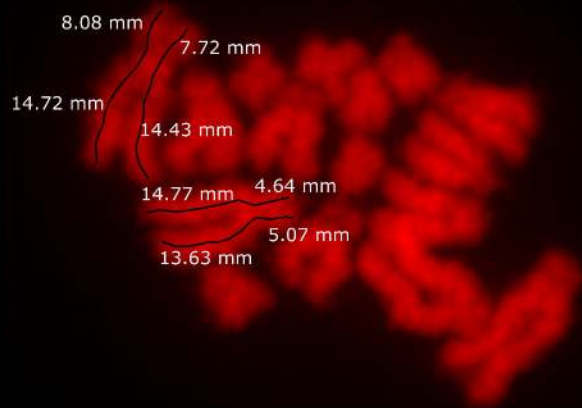
W016

- W005 ■
- W008 ■
- W010 ■
- W014 ■
- W012 ■
- W018 ■
- W017 ■
- W021 ■
- W022 ■
- W015 ■
- W023 ■

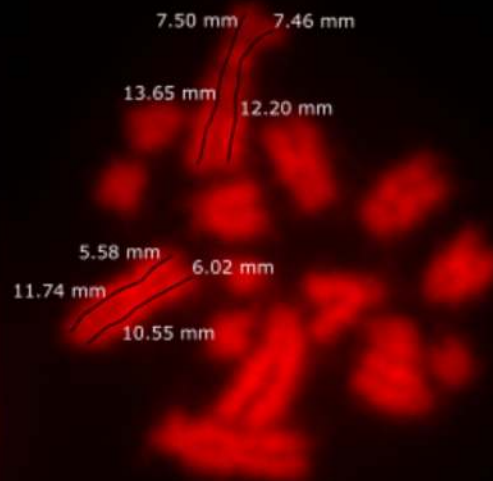
- W001
- W003
- W004
- W006
- W009
- W011
- W013
- W020
- 50kb



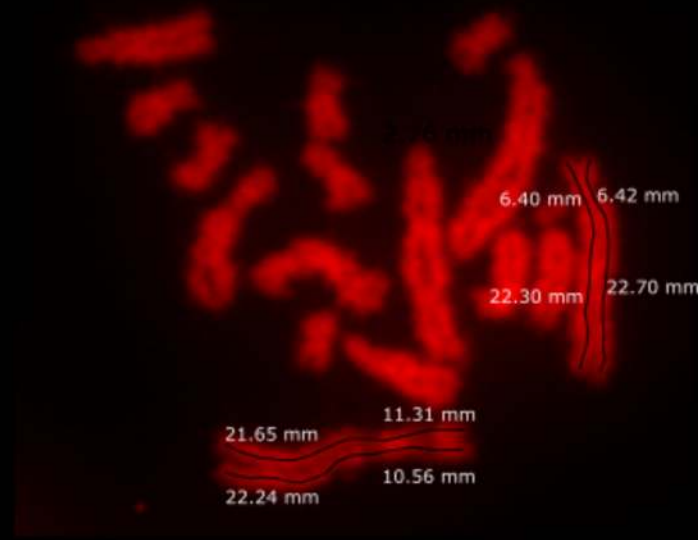
"Figure 1"



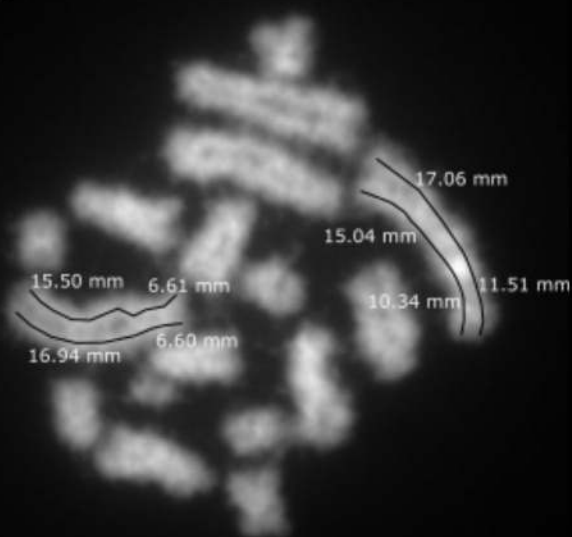
"Figure 5"



"Figure 7"



"Figure 8"



"Figure 9"

